CONTINUED DEVELOPMENT OF NODAL METHODS FOR NUCLEAR REACTOR ANALYSIS

by

A. Henry, A. Dias, W. Francis, A. Parlos,
E. Tanker, and Z. Tanker

MIT EL 86-002 June 1986

CONTINUED DEVELOPMENT OF NODAL METHODS

FOR NUCLEAR REACTOR ANALYSIS

Final Report for the Period March 1985 Through June 1986

Project Director: A. F. Henry
Work performed by: Antonio Dias
Winston Francis
Alex Parlos
Ediz Tanker
Zeynep Tanker

Energy Laboratory
and
Department of Nuclear Engineering

Massachusetts Institute of Technology
Cambridge, Massachusetts 02139

Sponsored by

Northeast Utilities Service Company
Pacific Gas & Electric Company

under the

M.I.T. Energy Laboratory Electric Utility Program

M.I.T. Energy Laboratory Report No. MIT-EL-86-002

June 1986

Table of Contents

Acknowledgments

The work described in this report was supported by Northeast Utilities Service Company and Pacific Gas and Electric Company under the MIT Energy Laboratory Electric Utility Program. We wish to express our thanks for that support.

Foreword

The physics design of nuclear reactors is today carried out, almost exclusively, by the application of numerical models that describe neutron behavior in a core throughout its life history. It is accordingly very important that the models used be accurate and reliable. At the same time, they must not require exorbitant amounts of computing machine time.

The present report is a summary of a third year of effort in an on-going program to improve such mathematical models. The development of improved procedures for analyzing static problems (including depletion and fuel management) has been quite successful and is now largely complete, and present concentration is on applications to transient analysis. Implementation of the methods developed into production computer programs that fit into presently used packages remains as the most important outstanding requirement.

Introduction

The development of computer programs that predict neutron behavior in nuclear reactors falls into three stages.

The first stage involves the derivation of the basic equations that constitute the model. These are best found by systematic reduction from a more accurate model so that the physical and mathematical approximations made can be understood clearly.

Next it is necessary to create a computer program that solves the model equations and to test its accuracy by comparison with reference calculations.

Finally, it is necessary to fit the tested model into standard production codes. It is really only when this last stage is complete that utilities can take advantage of the improved accuracy and efficiency of the newer models.

The MIT development is now reaching this final stage. Production codes based on the nodal code QUANDRY developed at MIT are now coming into use. These include the nodal option QPANDA of SIMULATE-3 developed by Studsvik of America, the STAR program developed at N.U.S., and the ARROTTA code developed at S. Levy for EPRI.

Some of these organizations have undertaken development work which might have been carried out at MIT. For examples, both Studsvik and N.U.S. have successfully incorporated into their nodal

codes an improved iteration scheme (suggested by Kord Smith) which reduces computer storage requirements substantially. In addition, Studsvik is providing a direct link between CASMO and QPANDA which avoids entirely the need to run any fine-mesh PDQ problems -- either assembly-sized or quarter-core -- in order to obtain homogenized nodal parameters. Finally, Temitope Taiwo, working at Northeast Utilities, has reprogrammed QUANDRY to solve for the nodal adjoint fluxes.

Since complex production-type programming efforts of this nature are better carried out by organizations where the personnel are not continually changing (as happens with graduate students), we were pleased to be able to drop these items from our agenda. Instead, we have continued to concentrate on the development and preliminary testing of accurate and efficient methods for predicting neutron behavior in LWRs. Accomplishments of the past year are described in the sections below.

To summarize briefly:

1) We have completed the development and testing of a method for determining fine-mesh, finite-difference, diffusion theory parameters (such as are used in PDQ) that reproduce quite accurately the criticality and power distribution produced by transport spectrum codes such as CPM or CASMO.

2) We have shown how to derive the adjustable parameters required by the standard nodal codes FLARE and PRESTO directly from a QUANDRY calculation.

3) All the necessary computer codes for testing a new scheme for reconstructing detailed pin-power distributions from QUANDRY solutions for BWR's have been completed.

4) A one-dimensional, two-group scheme for analyzing transient neutron behavior has been derived systematically from the QUANDRY, three-dimensional nodal equations. Coding is substantially complete, and testing has begun.

5) New time-integration schemes for solving the point kinetics equations, which permit the use of large time steps, have been developed and tested.

1. Transport Effects Accounted for by a Finite-Difference Diffusion Theory Model

We have completed the development of a systematic method for deriving few-group, fine-mesh, finite-difference diffusion theory parameters from multi-group, transport theory calculations carried out for an entire assembly.

A discussion of the theory along with a number of numerical test cases is given in MIT-EL-85-002,[1] and Reference (2) is a complete report of the work done on the method.

Face-dependent discontinuity factors for the pin-cells are initially introduced to reproduce the transport results exactly. With adjustments made for fuel cells adjacent to control rod fingers or burnable poison cells and for cells adjacent to the reflector, the face-dependent discontinuity factors can be replaced with approximate average values, and then, by a renormalization of the

two-group cross sections, can be made to disappear entirely. Thus, the standard finite difference code, PDQ, can be made to reproduce rather closely all the reaction rates determined by transport theory. Maximum errors in pin-power (relative to reference calculations) were under 2% for our test cases. Since the adjustments for cells next to a control finger or poison pin or reflector can be made automatic, the method is more straightforward than the trial-and-error procedure currently used by most utilities. Also, since all reaction rates are matched (rather than just absorption in burnable poison pins or control fingers, it is expected to be more accurate.

To illustrate the method for a difficult case, we consider the rodded assembly shown on Figure (1-1). The black squares represent fuel-pin-sized regions occupied by control rod fingers. Figure (1-2) shows an eighth of the assembly partitioned into three zones along with the legend for Figures (1-3), (1-4) and (1-5). These latter figures show, for the three partitions, the error in pin power when the "(3+1)" approximation (explained below) is used along with the average group-1 and 2 discontinuity factors and the face-dependent, group-1 and 2 discontinuity factors for each pin-sized region. The face-dependent discontinuity factors were found by requiring that "exact" finite-difference type equations with one mesh-square per pin-cell and incorporating three discontinuity factors (Ref. 1) reproduce reference results for the pin-cell-averaged group-fluxes. (For both reference and approximate

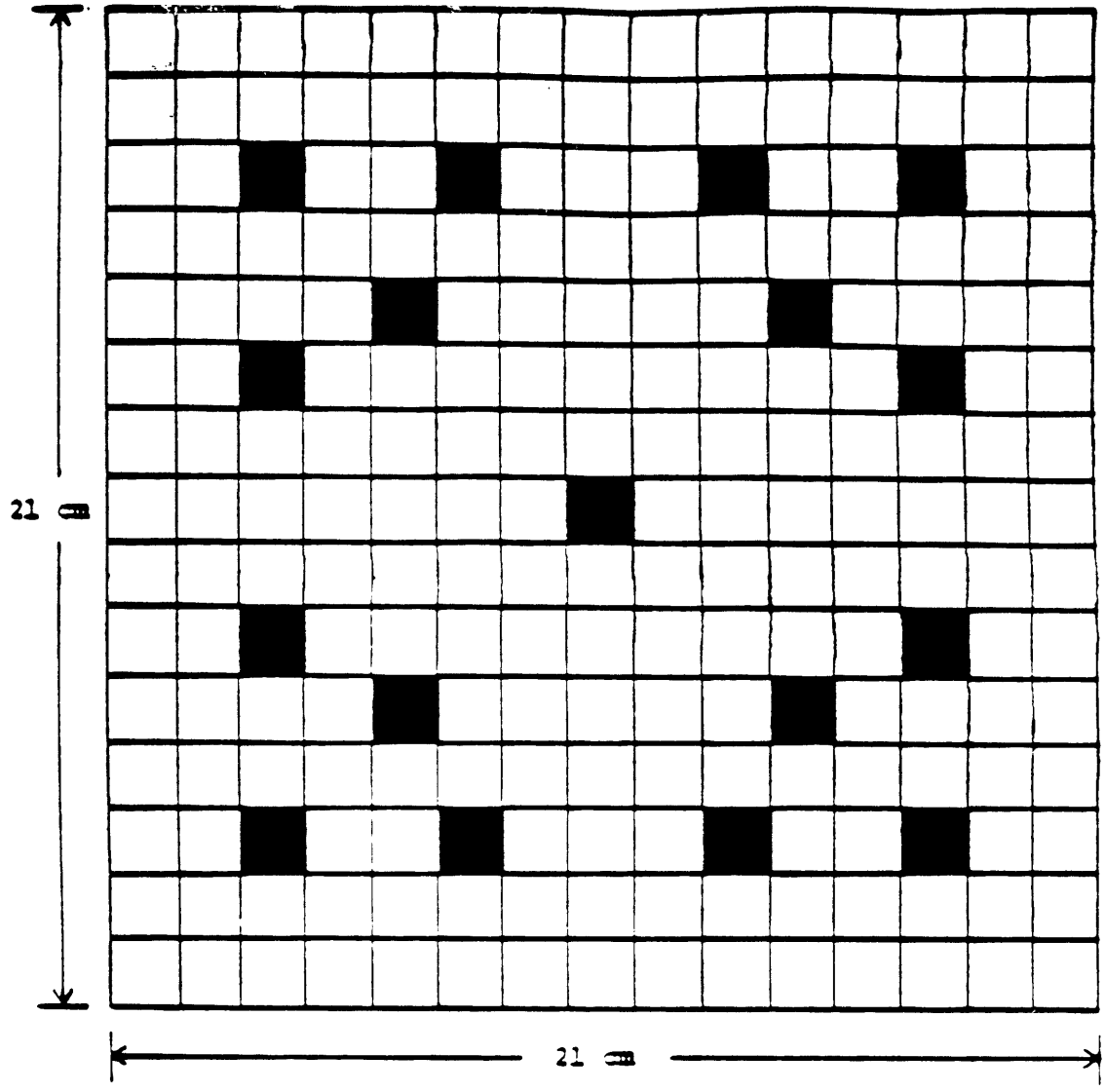

Fig. 1.1 Heterogeneous PWR Assembly Geometry

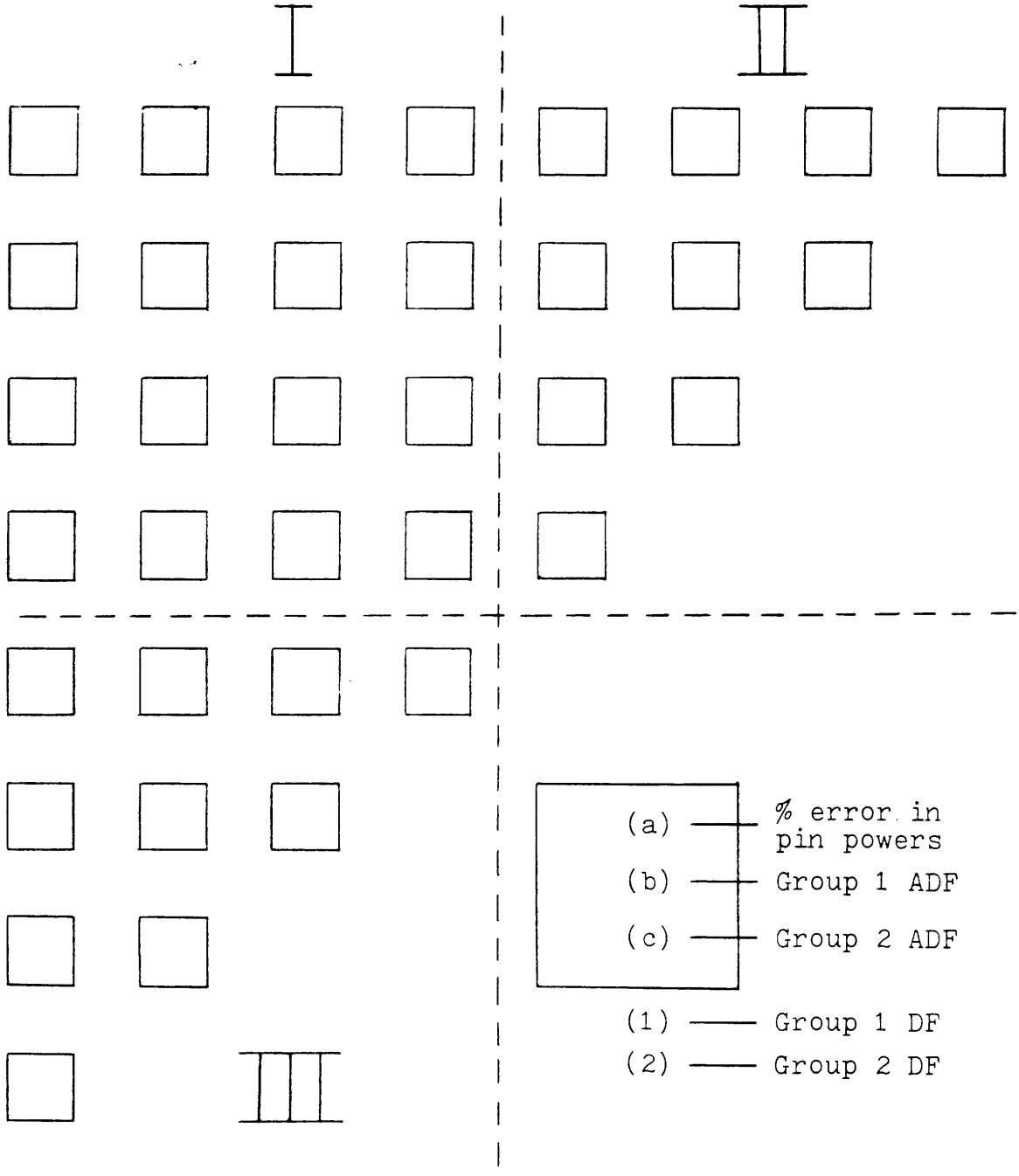

Fig. (1-2) - Rodded reference discontinuity factors, (3+1) averages and the errors in pin powers

Fig. (1-3) cont'd - Partition I

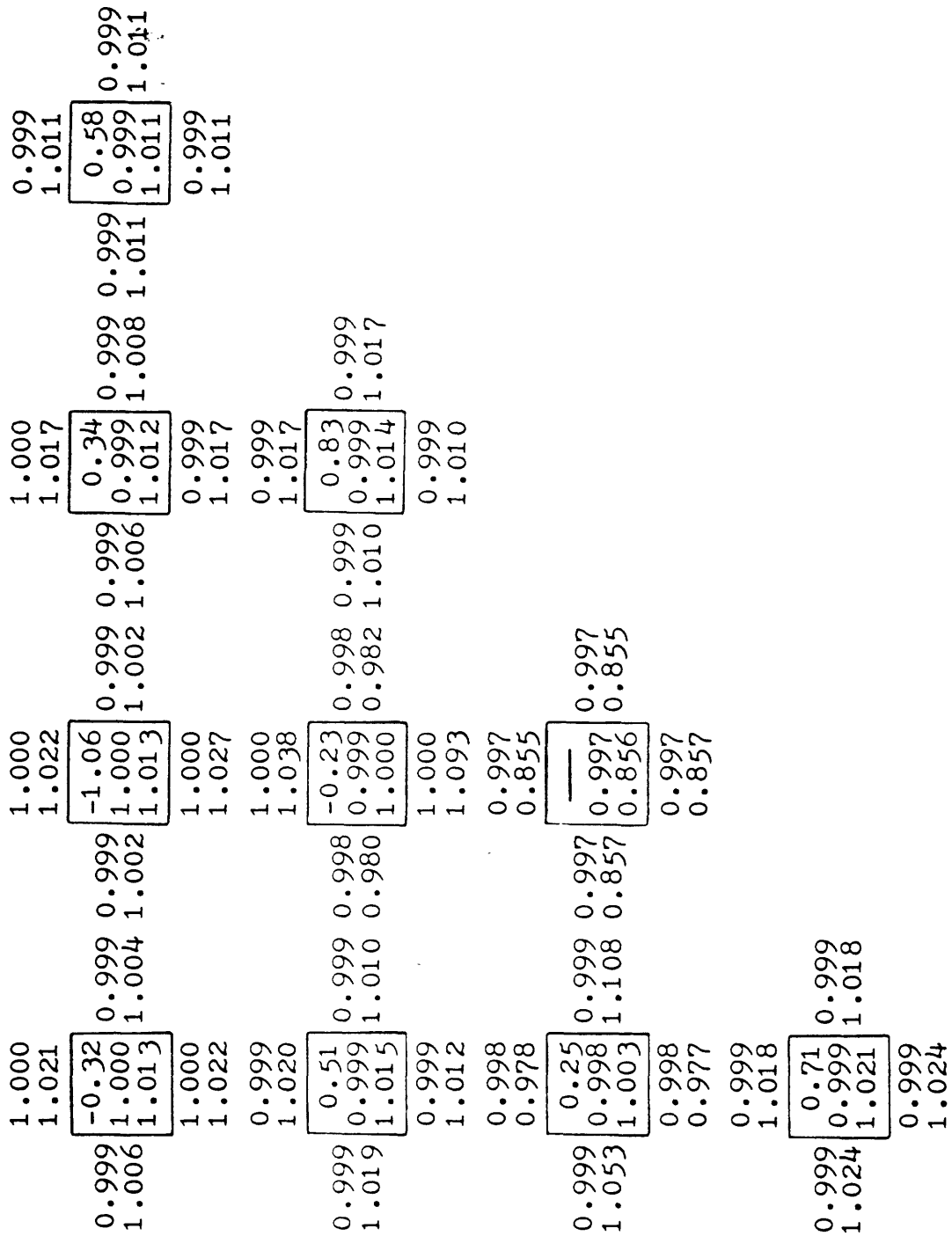

Fig. (1-4) cont'd - Partition II

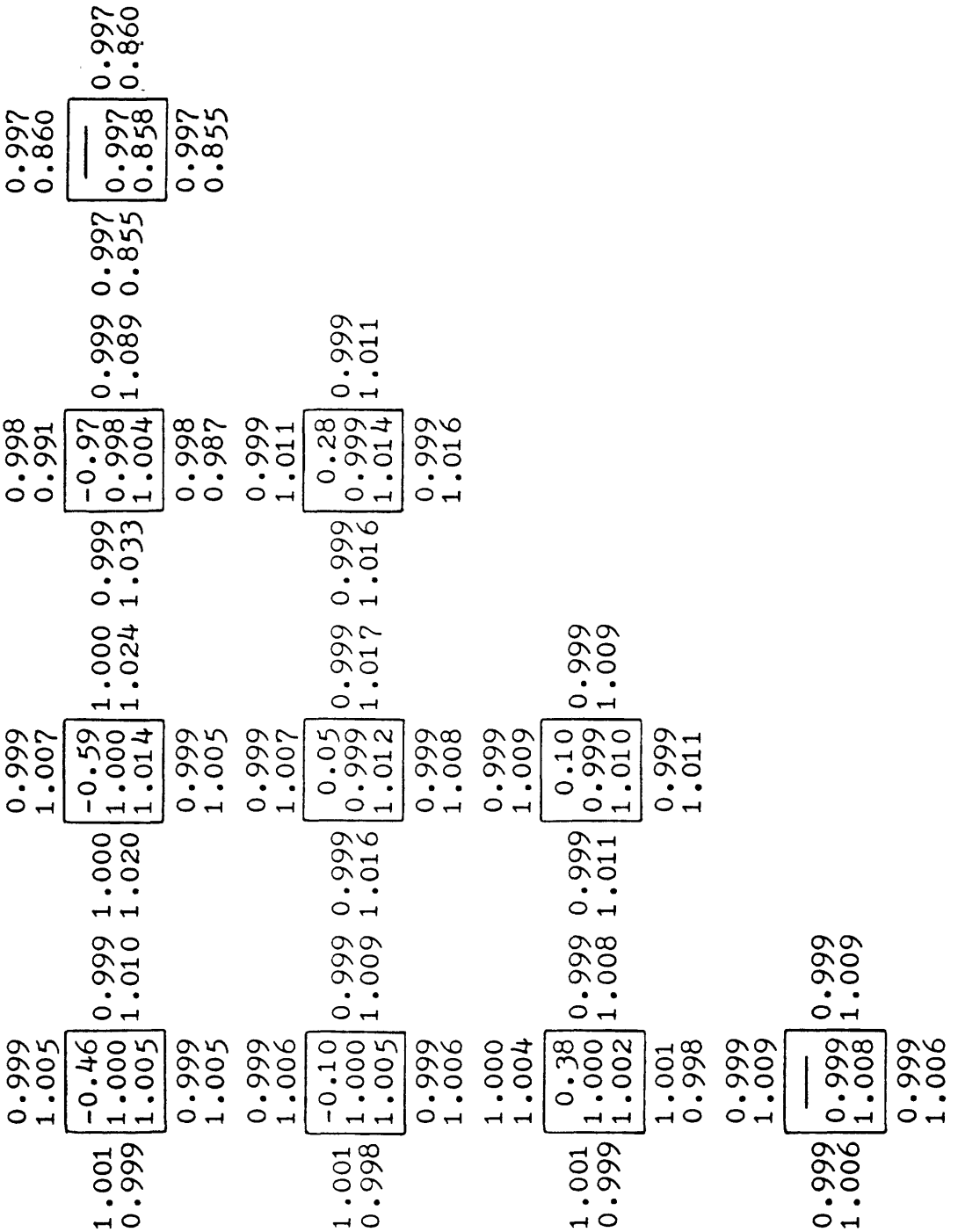

(Fig. (1-5) cont'd - Partition III

assembly calculations, zero-current boundary conditions were applied over the entire surface of the assembly.)

As shown in Ref. (1), if the face-dependent discontinuity factors are replaced by their cell-averaged values and if the homogenized diffusion coefficients and cross sections for the pin cells are divided by these average values, a set of finite difference equations similar to those used for standard design (PDQ) is obtained. Thus, insofar as face-dependent discontinuity factors may be replaced by average values, PDQ can be made to match CPM or CASMO results by a straightforward, one-step procedure.

Unfortunately, Figures 1-3), (1-4) and (1-5) show that, for the fuel-pin cells adjacent to rodded cells, the group-2 discontinuity factor for the face nearest the rod-finger is significantly higher than those of the other three faces. Thus, replacing the face-dependent, group-2 discontinuity factors of fuel-pin cells adjacent to rodded cells by average values is likely to be a poor approximation.

We have developed two methods to circumvent this difficulty. The first is to average (for fuel-pin cells adjacent to a rodded cell) the thermal discontinuity factors for only the <u>three</u> faces <u>furthest</u> from the rodded cell and to use the actual face-dependent value for the faces nearest the rodded cell. This is the "(3+1)" approximation.

The second scheme is based on the fact that what appears in the "exact" finite difference equations is the ratio of the

discontinuity factors on the two sides of that interface. Examination of Fig. (1-3) shows that the face dependent, group-2 discontinuity factors for the rodded cell vary in the narrow range 0.855 to 0.857, and those for the faces which the four neighboring fuel-pin cells have in common with the rodded cell vary in the range 1.093-1.106. Moreover, for the four fuel-pin cells adjacent to the rodded cell, the averages of the thermal discontinuity factors for the three faces not common with those of the rodded cell vary in the range 0.999 to 1.004. It follows that if we reduce the thermal discontinuity factors of the faces adjacent to the rodded cell and those of the rodded cell by dividing by, say, 1.1, the ratio of discontinuity factors across faces will be unaltered, but the values of all four thermal discontinuity factors for fuel-pin cells adjacent to the rodded cell will be much closer to each other, so that replacing them by their average value will be a much better approximation. We call discontinuity factors altered in this manner "adjusted discontinuity factors."

Table (1-1) shows the difference from reference results due to the use of various averaging procedures applied to the discontinuity factors of the pin-sized-cells comprising the assembly of Figure (1-1). Clearly, using unity-valued discontinuity factors (no correction) leads to unacceptable errors in both eigenvalue and pin-power. Straight arithmetically-averaged discontinuity factors do little better. (Tests presented in Ref. (1) show that arithmetically-averaged discontinuity factors do well when water

	k_{eff}	% error in k_{eff}	Max. % error in pin powers
Reference	0.890886	0.0	0.0
Unity DFs	0.934427	4.89	5.28
Arithmetic average DFs	0.906057	1.70	-3.47
f_{gx} and f_{gy} averaged separately	0.896418	0.62	-1.45
(3+1) DFs	0.891307	0.05	-1.83
Adjusted DFs	0.89120	0.04	1.80

Table (1-1) - Rodded Preliminary Calculations

holes rather than control rod fingers are present.) Use of separate averages for the x and y directions leads to the smallest error in predicted fuel-pin power, but an unacceptably large error in eigenvalue. On the other hand, both the (3+1) and the "adjusted" discontinuity factors do well.

Since the "adjusted" DF's can be made to disappear entirely by renormalization of the pin-cell cross sections, we recommend this as the favored method for forcing a match between PDQ and codes like CPM or CASMO.

2. Standard Nodal Codes Derived Systematically - Winston H. G. Francis

Standard nodal codes such as EPRI-NODE-P/B, FLARE or PRESTO usually require that certain adjustable parameters and albedos be determined by fitting to quarter-core PDQ results. Under the assumption that the discontinuity factors (6 per node, per energy group), which make fluxes predicted using the coarse mesh finite difference (CMFD) QUANDRY equations match exactly those obtained by the regular QUANDRY equations, can be replaced by one, average value per group, we show below that these standard models can be derived directly from QUANDRY. If this basic approximation is valid, "coupling constants" and albedos for the simple models can be found in a direct, non-iterative fashion.

To show how the fitted parameters of standard nodal schemes can be found directly from a QUANDRY solution, we shall first derive two of them (FLARE and PRESTO) in a standard fashion. Then we shall

show that, by using node-face-dependent discontinuity factors, finite-difference equations capable of reproducing reference QUANDRY results can be derived. The face-dependent discontinuity factors will then be approximated by node-averaged values, and the fitted parameters of FLARE and PRESTO will be found in terms of these averaged-values. Finally, we shall present some preliminary tests of the systematically derived FLARE and PRESTO models.

2.1 SEMI-EMPIRICAL NODAL METHODS

Semi-empirical nodal methods may be derived from the following multi-group equations[3],

$$\nabla\cdot\underline{J}_g(\underline{r}) + \Sigma_{tg}(\underline{r})\,\varphi_g(\underline{r})$$

$$= \sum_{g'=1}^{G} \left[\frac{1}{\lambda}\,\chi_g \nu\Sigma_{fg'}(\underline{r}) + \Sigma_{gg'}(\underline{r}) \right] \varphi_{g'}(\underline{r}) \qquad (2.1)$$

where the notation is conventional.

We consider a node (i,j,k), with a horizontal mesh spacing h in both the x- and y- directions, and a vertical mesh spacing k in the z-direction. By integrating over the volume of the node (i,j,k), and using Gauss' theorem, we obtain

$$\sum_{m=1}^{6} \int_{S_m} \underline{J}_g(\underline{r})\cdot\underline{n}_{S_m}\, dS + h^2 k\, \Sigma_{tg}^{i,j,k}\, \varphi_g^{i,j,k}$$

$$= h^2 k \sum_{g'=1}^{G} \left[\frac{1}{\lambda}\,\chi_g \nu\Sigma_{fg'}^{i,j,k} + \Sigma_{gg'}^{i,j,k} \right] \varphi_{g'}^{i,j,k} \qquad (2.2)$$

$$g = 1,2,\ldots,G.$$

We also divide the energy spectrum into two groups by setting $G = 2$, such that all fission neutrons are introduced into the fast group only, in which case $\chi_1 = 1$ and $\chi_2 = 0$, and there is no up-scattering, i.e. $\Sigma_{12}^{i,j,k} = 0$. For simplicity a generalized node (i,j,k) will be represented

by a single index "p", so that the resultant two-group equations are:

$$\sum_{m=1}^{6} \int_{S_m} \underline{J}_1(\underline{r}) \cdot \underline{n}_{S_m} \, dS + h^2 k \, \Sigma_1^p \, \varphi_1^p = \frac{h^2 k}{\lambda} \left[\nu\Sigma_{f1}^p \, \varphi_1^p + \nu\Sigma_{f2}^p \, \varphi_2^p \right] \tag{2.3a}$$

$$\sum_{m=1}^{6} \int_{S_m} \underline{J}_2(\underline{r}) \cdot \underline{n}_{S_m} \, dS + h^2 k \, \Sigma_2^p \, \varphi_2^p = h^2 k \, \Sigma_{21}^p \tag{2.3b}$$

where $\Sigma_1 \equiv \Sigma_{t1} - \Sigma_{11}$, and $\Sigma_2 \equiv \Sigma_{t2} - \Sigma_{22}$.

In the second (thermal) group, the leakage term is generally much smaller than the absorption term, and hence may be neglected. The result is the one-and-a-half group approximation. Alternatively, in order to maintain a formally exact scheme, we can define a parameter B_p^2, such that

$$\sum_{m=1}^{6} \int_{S_m} \underline{J}_2(\underline{r}) \cdot \underline{n}_{S_m} \, dS \equiv h_2 k \, D_2^p \, B_p^2 \, \varphi_2^p \tag{2.4}$$

so that

$$\varphi_2^p = \frac{\Sigma_{21}^p}{D_2^p \, B_p^2 + \Sigma_2^p} \, \varphi_1^p \tag{2.5}$$

The advantage of introducing B_p^2 will be apparent later, and obviously by setting $B_p^2 = 0$, we can return to the one-and-a-half group approximation. By using this relation between the φ_2^p and φ_1^p, we have essentially

reduced the problem to a one-group model, in which we only have to consider the fast group explicitly.

$$\sum_{m=1}^{6} \int_{S_m} \underline{J}_1(\underline{r}) \cdot \underline{n}_{S_m} \, dS + h^2 k \, \Sigma_1^p \, \varphi_1^p = \frac{h^2 k}{\lambda} \left[\nu\Sigma_{f1}^p + \nu\Sigma_{f2}^p \frac{\varphi_2^p}{\varphi_1^p} \right] \varphi_1^p$$

$$= \frac{h^2 k}{\lambda} \Sigma_1^p \, k_\infty^p \, \varphi_1^p \qquad (2.6)$$

$$k_\infty^p \equiv \frac{\nu\Sigma_{f1}^p}{\Sigma_1^p} + \frac{\nu\Sigma_{f2}^p \, \Sigma_{21}^p}{\Sigma_1^p \, (D_2^p \, B_p^2 + \Sigma_2^p)} \qquad (2.7)$$

where k_∞^p is the conventional infinite multiplication factor for a two-group model, with the materials buckling $(B_m^2)_p$ replaced by B_p^2 .

FLARE MODEL

In order to derive the FLARE model[4], we now define a fission neutron source term for each node,

$$S^p \equiv h^2 k \, \Sigma_1^p \, k_\infty^p \, \varphi_1^p \qquad (2.8)$$

so that Eq. 2.6 can be written

$$\sum_{q=1}^{6} \left[J^{p \to q} - J^{q \to p} \right] + \frac{S^p}{k_\infty^p} = \frac{S^p}{\lambda} \qquad (2.9)$$

where $J^{p \to q}$ represents the leakage from node p to an adjacent node q.

Rearrangement yields

$$S^p = \frac{k_\infty^p}{\lambda} \left[S^p - \lambda \sum_{q=1}^{6} \left[J^{p\to q} - J^{q\to p} \right] \right]$$

$$= \frac{k_\infty^p}{\lambda} \left[\left[1 - \sum_{q=1}^{6} \frac{J^{p\to q}}{\frac{1}{\bar{\lambda}} S^p} \right] S^p + \left[\sum_{q=1}^{6} \frac{J^{q\to p}}{\frac{1}{\bar{\lambda}} S^q} \right] S^q \right] \qquad (2.10)$$

By defining a kernel W^{pq} by the relation

$$W^{pq} \equiv \frac{J^{p\to q}}{\frac{1}{\bar{\lambda}} S^p} \qquad (2.11)$$

so that W^{pq} represents approximately the probability that a neutron in node p in a reactor, which is artifically critical, will cross to an adjacent node q, we may rewrite Eq.2.10 as

$$S^p = \frac{k_\infty^p}{\lambda} \left[\left[1 - \sum_{q=1}^{6} W^{pq} \right] S^p + \sum_{q=1}^{6} W^{qp} S^q \right] \qquad (2.12)$$

which is the basic nodel equation in the FLARE model.

In FLARE, the kernel W^{pq} is taken to be of the form[4]:

$$W^{pq} = (1 - g) \frac{\rfloor(M_p^2)}{2h} + g \frac{M_p^2}{h^2} \qquad (2.13)$$

where g is an adjustable parameter, and M_p^2 is the migration area.

According to this expression, W^{pq} depends only on the properties of node p, a condition which is obviously not true physically. The kernel was originally derived as a combination of a slab-diffusion kernel and a difference-equation kernel in a non-rigorous and quite arbitrary manner. However, by adjustment of the g-factor and the albedos, it is possible to reproduce a reference solution, i.e. eigenvalue λ to < 0.5 % and the nodal powers to < 10%, which is considered satisfactory for initial design calculations.

PRESTO MODEL

The PRESTO model[5] is a modified coarse-mesh finite-difference (MCMFD) model, which uses node-centred and face-centred point fluxes. The nodal volume-averaged flux is assumed to be approximated by

$$\bar{\varphi}^p \simeq \frac{3a}{3a+(1-a)(R+2)}\varphi^p + 2\frac{(1-a)/4}{3a+(1-a)(R+2)}\left[\sum_{q_h=1}^{4}\varphi^{pq} + R\sum_{q_v=1}^{2}\varphi^{pq}\right] \qquad (2.14)$$

where φ^p is the point flux at the center of node p, and φ^{pq} is the center-point flux on the interface between nodes p and an adjacent node q, with "a" being an adjustable weighting factor. We note that when $R = h^2/k^2 = 1$, i.e. h = k

$$\bar{\varphi}^p \simeq a\,\varphi^p + \frac{1-a}{6}\sum_{q=1}^{6}\varphi^{pq} \qquad (2.15)$$

Introducing the definition (2.7) into the fast group equation (2.3a) yields

$$\sum_{m=1}^{6} \int_{S_m} \underline{J}_1(\underline{r}) \cdot \underline{n}_{S_m} \, dS = h^2 k \left[\frac{1}{\lambda} k_\infty^p - 1 \right] \Sigma_1^p \, \bar{\varphi}_1^p \tag{2.16}$$

where φ_1^p is replaced by $\bar{\varphi}_1^p$ to distinguish point fluxes from nodal volume-averaged fluxes. In order to determine the left-hand-side, the net current on the interface between adjacent nodes p and q is assumed to be given by

$$J^{pq} \simeq - D^p \left[\frac{\varphi^{pq} - \varphi^p}{h/2} \right]$$

$$\simeq - D^q \left[\frac{\varphi^q - \varphi^{pq}}{h/2} \right] \tag{2.17}$$

With this assumption made, the surface fluxes and currents on the interface are

$$\varphi^{pq} \simeq \frac{D^p \varphi^p + D^q \varphi^q}{D^p + D^q} \tag{2.18}$$

$$J^{pq} \simeq - \frac{2}{h} \frac{D^p D^q}{D^p + D^q} (\varphi^q - \varphi^p) \tag{2.19}$$

Hence Eq. (2.16) becomes

$$\sum_{q_h=1}^{4} -(hk)\,\frac{2}{h}\,\frac{D^p\,D^q}{D^p+D^q}\,(\varphi^q-\varphi^p) + \sum_{q_v=1}^{2} -(h^2)\,\frac{2}{k}\,\frac{D^p\,D^q}{D^p+D^q}\,(\varphi^q-\varphi^p)$$

$$= h^2k\left[\frac{1}{\lambda}\,k_\infty^p - 1\right]\Sigma^p\,\bar{\varphi}^p \qquad (2.20)$$

where the subscript for group-1 has been dropped, so that

$$\sum_{q_h=1}^{4} -2k\,\frac{D^p\,D^q}{D^p+D^q}\,(\varphi^q-\varphi^p) - \sum_{q_v=1}^{2} 2kR\,\frac{D^p\,D^q}{D^p+D^q}\,(\varphi^q-\varphi^p)$$

$$= h^2k\left[\frac{1}{\lambda}\,k_\infty^p - 1\right]\Sigma^p\,\bar{\varphi}^p$$

$$= h^2k\left[\frac{1}{\lambda}k_\infty^p - 1\right]\Sigma^p\left[\frac{3a}{3a+(1-a)(R+2)}\,\varphi^p + 2\,\frac{(1-a)/4}{3a+(1-a)(R+2)}\left[\sum_{q_h=1}^{4}\varphi^{pq} + R\sum_{q_v=1}^{2}\varphi^{pq}\right]\right] \qquad (2.21)$$

This set of equations, together with suitable boundary conditions, can be solved to yield the point fluxes φ^p, from which the nodal-averaged fluxes can then be reconstructed.

2.2 SYSTEMATIC NODAL METHODS

The starting point of all nodal methods based on diffusion theory is the set of multi-group equations (2.1), which is repeated here

$$\nabla\cdot\underline{J}_g(\underline{r}) + \Sigma_{tg}(\underline{r})\,\varphi_g(\underline{r})$$

$$= \sum_{g'=1}^{G}\left[\frac{1}{\lambda}\chi_g\nu\Sigma_{fg'}(\underline{r}) + \Sigma_{gg'}(\underline{r})\right]\varphi_{g'}(\underline{r}) \qquad (2.22)$$

We again consider a node (i,j,k), with a horizontal mesh spacing "h" in both the x- and y- directions, and a vertical mesh spacing "k" in the z-direction. Integrating Eq. (3.1) over the volume of the node (i,j,k), we again obtain

$$\sum_{m=1}^{6}\int_{S_m}\underline{J}_g(\underline{r})\cdot\underline{n}_{S_m}\,dS + h^2k\,\Sigma_{tg}^{i,j,k}\,\varphi_g^{i,j,k}$$

$$= h^2k\sum_{g'=1}^{G}\left[\frac{1}{\lambda}\chi_g\nu\Sigma_{fg'}^{i,j,k} + \Sigma_{gg'}^{i,j,k}\right]\varphi_{g'}^{i,j,k} \qquad (2.23)$$

$$g = 1,2,\ldots,G.$$

Since Eq. (2.23) contains two unknowns φ_g^{ijk} and $\underline{J}_g(\underline{r})$, we require another relation between them, so as to form a closed set of equations. This relation is usually termed the "nodal coupling equation", and is mainly responsible for the differences in the various nodal methods.

ANALYTIC NODAL METHOD (QUANDRY-CMFD APPROXIMATION)

In the CMFD approximation, the nodal coupling equation is based on Fick's law of diffusion

$$\int\int J_{gx}(x_{i+1},y,z)\,dy\,dz$$

$$\simeq -D_g^{i+1,j,k}\,\frac{hk\,\varphi_g^{i+1,j,k} - \frac{1}{f_{gx-}^{i+1,j,k}}\int\int \varphi_g(x_{i+1},y,z)\,dy\,dz}{h/2}$$

$$\simeq -D_g^{i,j,k}\,\frac{\frac{1}{f_{gx+}^{i,j,k}}\int\int \varphi_g(x_{i+1},y,z)\,dy\,dz - hk\,\varphi_g^{i,j,k}}{h/2} \qquad (2.24)$$

where because of the introduction of the discontinuity factors $f_{gx-}^{i+1,j,k}$ and $f_{gx+}^{i,j,k}$, these are now formally exact relations. (To put it another way, Equa. (2.24) defines formally exact values for the discontinuity factors.)

Eliminating the face integrated surfaces from Equa. (2.24) yields

$$\int\int J_{gx}(x_{i+1},y,z)\,dy\,dz$$

$$= -2k\,\frac{D_g^{i,j,k}\,D_g^{i+1,j,k}}{f_{gx+}^{i,j,k}D_g^{i+1,j,k} + f_{gx-}^{i+1,j,k}D_g^{i,j,k}}\left[\,f_{gx-}^{i+1,j,k}\varphi_g^{i+1,j,k} - f_{gx+}^{i,j,k}\varphi_g^{i,j,k}\,\right]$$

$$= -2k\left[\frac{f_{gx-}^{i+1,j,k}}{D_g^{i+1,j,k}} + \frac{f_{gx+}^{i,j,k}}{D_g^{i,j,k}}\right]^{-1}\left[\,f_{gx-}^{i+1,j,k}\varphi_g^{i+1,j,k} - f_{gx+}^{i,j,k}\varphi_g^{i,j,k}\,\right] \qquad (2.25)$$

Similar expressions can be obtained for $\int\int J_{gx}(x_i,y,z)\,dy\,dz$, $\int\int J_{gy}(x,y_{j+1},z)\,dz\,dx$, etc. By introducing these expressions into equation (1.24), the QUANDRY-CMFD equations are obtained,

$$- 2k \left[\frac{f_{gx-}^{i+1,jk}}{D_g^{i+1,jk}} + \frac{f_{gx+}^{ijk}}{D_g^{ijk}} \right]^{-1} \left[f_{gx-}^{i+1,jk} \varphi_g^{i+1,jk} - f_{gx+}^{ijk} \varphi_g^{ijk} \right]$$

$$+ 2k \left[\frac{f_{gx+}^{i-1,jk}}{D_g^{i-1,jk}} + \frac{f_{gx-}^{ijk}}{D_g^{ijk}} \right]^{-1} \left[f_{gx-}^{ijk} \varphi_g^{ijk} - f_{gx+}^{i-1,jk} \varphi_g^{i-1,jk} \right]$$

$$- 2k \left[\frac{f_{gy-}^{i,j+1,k}}{D_g^{i,j+1,k}} + \frac{f_{gy+}^{ijk}}{D_g^{ijk}} \right]^{-1} \left[f_{gy-}^{i,j+1,k} \varphi_g^{i,j+1,k} - f_{gy+}^{ijk} \varphi_g^{ijk} \right]$$

$$+ 2k \left[\frac{f_{gy+}^{i,j-1,k}}{D_g^{i,j-1,k}} + \frac{f_{gy-}^{ijk}}{D_g^{ijk}} \right]^{-1} \left[f_{gy+}^{ijk} \varphi_g^{ijk} - f_{gy-}^{i,j-1,k} \varphi_g^{i,j-1,k} \right]$$

$$- \frac{2h^2}{k} \left[\frac{f_{gz-}^{ij,k+1}}{D_g^{ij,k+1}} + \frac{f_{gz+}^{ijk}}{D_g^{ijk}} \right]^{-1} \left[f_{gz-}^{ij,k+1} \varphi_g^{ij,k+1} - f_{gz+}^{ijk} \varphi_g^{ijk} \right]$$

$$+ \frac{2h^2}{k} \left[\frac{f_{gz+}^{ij,k-1}}{D_g^{ij,k-1}} + \frac{f_{gz-}^{ijk}}{D_g^{ijk}} \right]^{-1} \left[f_{gz-}^{ijk} \varphi_g^{ijk} - f_{gz+}^{ij,k-1} \varphi_g^{ij,k-1} \right]$$

$$+ h^2 k \, \Sigma_g^{i,j,k} \varphi_g^{i,j,k} = h^2 k \sum_{g'=1}^{G} \left[\frac{1}{\lambda} \chi_g \nu \Sigma_{fg'}^{i,j,k} + \Sigma_{gg'}^{i,j,k} \right] \varphi_{g'}^{i,j,k} \qquad (2.26)$$

It may be noted that these equations have a more general structure than the conventional finite-difference equations used in PDQ[6] and CITATION[7], where the discontinuity factors are implicitly taken as unity.

2.3. FLARE MODEL: REDUCTION OF QUANDRY-CMFD EQUATIONS

In order to reduce equation (2.26) to the FLARE equations, which are based on a one-group model, we first set G = 1, and define

$$S^{i,j,k} = h^2 k \, \Sigma_g^{i,j,k} \, k_\infty^{i,j,k} \, \varphi_g^{i,j,k} \tag{2.27}$$

where, $k_\infty^{i,j,k} = \nu\Sigma_f^{i,j,k} \; / \; \Sigma^{i,j,k}$ (2.28)

Then the QUANDRY-CMFD equations may be written,

$$S^{ijk} = \frac{k_\infty^{ijk}}{\lambda}\Bigg[\Bigg[1 - \frac{2k\lambda}{h^2 k \Sigma^{ijk} k_\infty^{ijk}}\left[\frac{f_{x+}^{ijk}}{\frac{f_{x-}^{i+1,jk}}{D^{i+1,jk}} + \frac{f_{x+}^{ijk}}{D^{ijk}}}\right] - \frac{2k\lambda}{h^2 k \Sigma^{ijk} k_\infty^{ijk}}\left[\frac{f_{x-}^{ijk}}{\frac{f_{x-}^{ijk}}{D^{ijk}} + \frac{f_{x+}^{i-1,jk}}{D^{i-1,jk}}}\right]$$

$$- \ldots\ldots\ldots\ldots\ldots\ldots\Bigg] S^{ijk}$$

$$+ \frac{2k\lambda}{h^2 k \Sigma^{i+1,jk} k_\infty^{i+1,jk}}\left[\frac{f_{x-}^{i+1,jk}}{\frac{f_{x-}^{i+1,jk}}{D^{i+1,jk}} + \frac{f_{x+}^{ijk}}{D^{ijk}}}\right] S^{i+1,jk} + \ldots$$

$$\ldots + \frac{2\,(h^2/k)\,\lambda}{h^2 k \Sigma^{ij,k-1} k_\infty^{ij,k-1}}\left[\frac{f_{z+}^{ij,k-1}}{\frac{f_{z+}^{ij,k-1}}{D^{ij,k-1}} + \frac{f_{z-}^{ijk}}{D^{ijk}}}\right] S^{ij,k-1}\Bigg] \tag{2.29a}$$

$$= \frac{k_\infty^{i,j,k}}{\lambda} \left[\left[1 - W^{i,j,k\to i+1,j,k} - W^{i,j,k\to i-1,j,k} - \ldots \right] S^{i,j,k} \right.$$

$$\left. + W^{i+1,j,k\to i,j,k}\, S^{i+1,j,k} + \ldots + W^{i,j,k-1\to i,j,k}\, S^{i,j,k-1} \right] \tag{2.29b}$$

where

$$W^{i,j,k\to i+1,j,k} = \frac{2k\lambda}{h^2 k\, \Sigma^{i,j,k}\, k_\infty^{i,j,k}} \left[\frac{f_{x+}^{i,j,k}}{\frac{f_{x-}^{i+1,j,k}}{D^{i+1,j,k}} + \frac{f_{x+}^{i,j,k}}{D^{i,j,k}}} \right] \tag{2.30}$$

and hence in the form of the FLARE equations, i.e.

$$S^p = \frac{k_\infty^p}{\lambda} \left[\left[1 - \sum_{q=1}^{6} W^{pq} \right] S^p + \sum_{q=1}^{6} W^{qp}\, S^q \right] \tag{2.31}$$

where p represents the indices i,j,k of the node (i,j,k), and q represents the indices (i±1,j±1,k±1) of an adjacent node, so that in general,

$$W^{pq} = \frac{2\,\lambda}{(\,\Delta u\,)^2\, \Sigma^p\, k_\infty^p} \left[\frac{f_{u\pm}^p}{\frac{f_{u\pm}^p}{D^p} + \frac{f_u^q}{D^q}} \right] \tag{2.32}$$

In FLARE, the kernel W^{pq} is assumed to be of the form,

$$W^{pq} = (1 - g) \frac{\lfloor (M_p^2)}{2h} + g \frac{M_p^2}{h^2} \tag{2.33}$$

where g is an adjustable parameter, and M_p^2 is the migration area,

$$M_p^2 \equiv \frac{D_1^p}{\Sigma_1^p} + \frac{D_2^p}{\Sigma_2^p} \tag{2.34}$$

so that

$$g = \frac{W^{qp} - \lfloor (M_p^2)/2h}{M_p^2/h^2 - \lfloor (M_p^2)/2h} \tag{2.35}$$

From this it is immediately apparent that g should actually be a face-dependent parameter, i.e. $g \rightarrow g_{pq}$,where

$$g_{pq} = \frac{\frac{2\lambda}{(\Delta u)^2 \Sigma^p k_\infty^p} \left[\frac{f_{u\pm}^p}{\frac{f_{u\pm}^p}{D^p} + \frac{f_u^q}{D^q}} \right] - \frac{\lfloor (M_p^2)}{2(\Delta u)}}{\frac{M_p^2}{(\Delta u)^2} - \frac{\lfloor (M_p^2)}{2(\Delta u)}} \tag{2.36}$$

A basic limitation in FLARE is due to replacing g_{pq} by a single g-factor, or as is actually the case, by a g_h-factor for horizontal coupling and a g_v-factor for vertical coupling. This results in the kernel

W^{pq} being the same for all adjacent nodes in a horizontal plane, which implies that the probability that a neutron born in node p being ultimately absorbed in node q is the same for all adjacent horizontal nodes. While the error due to this approximation may be small for nodes in the interior of a reactor, it can be very large for nodes on the boundary, where the ratio $W^{pq} / W^{pq'}$ is significantly greater than unity. One way in which FLARE overcomes this problem is by arbitrarily adjusting the albedos, as well as the g-factor.

It is evident that if FLARE were modified to use face-dependent g_{pq}-factors and node-dependent albedos, the results would reproduce exactly the reference solution. However, as previously stated the purpose of this research is to determine systematically the arbitrary parameters, i.e. the g-factors and the albedos, which would allow the present FLARE program (perhaps modified to include node-dependent g_p-factors) to reproduce the reference results.

RELATION BETWEEN ALBEDOS IN QUANDRY AND FLARE

A relation between the albedos in QUANDRY and FLARE can be obtained by two approaches, which are essentially equivalent.In the first method, the total albedo for a node is obtained by introducing the conventional form of the FLARE equation[4],

$$S^p = \frac{k_\infty^p}{\lambda} \left[\left[1 - (6 - \alpha_{F(Tot)}^p) \bar{W}^{pq} \right] S^p + \sum_{q \neq q'} \bar{W}^{qp} S^q \right] \qquad (2.37)$$

where $\alpha^{p}_{F(Tot)}$ is the total albedo for any node p; q represents any of the nearest neighbours (maximum = six) which are present, and q′ any "missing" neighbours, if node p has one or more exterior surfaces. The exact form of the above equation using face-dependent kernels W^{pq} may be written in the form:

$$S^{p} = \frac{k^{p}_{\infty}}{\lambda} \left[\left[1 - \sum_{q \neq q'} W^{pq} - \sum_{q'} W^{pq'} \right] S^{p} + \sum_{q \neq q'} W^{qp} S^{q} \right] \qquad (2.38)$$

By equating the terms

$$(6 - \alpha^{p}_{F(Tot)}) \bar{W}^{pq} = \sum_{q \neq q'} W^{pq} + \sum_{q'} W^{pq'}$$

so that

$$\alpha^{p}_{F(Tot)} = 6 - \frac{\sum_{q \neq q'} W^{pq} + \sum_{q'} W^{pq'}}{\bar{W}^{pq}} \qquad (2.39)$$

a total FLARE albedo $\alpha^{p}_{F(Tot)}$ for node-p is obtained for any $\bar{W}^{pq}$ calculated using a node-dependent g_p and Equa. (2.33). While the coefficient of the S^{p} term is now exact, the exact S^{q} coefficients W^{qp} are replaced by $\bar{W}^{qp}$. In order to make these more nearly equal, the node-dependent g_p's should be averaged only over the interfaces with other nodes, excluding all albedo surfaces.

In the second approach, we consider a single exterior node face or albedo surface at a time, and equate the net leakages given by the QUANDRY-CMFD and FLARE models. For a first-order finite-difference approximation, the net surface current (leakage) at $x = x_{l+1}$ for group-g in the QUANDRY-CMFD model is

$$L_g^{i,j,k\to i+1,j,k} \equiv \int\int J_{gx}(x_{i+1},y,z)\, dy\, dz$$

$$= D_g^{i,j,k} \left[\frac{\frac{1}{f_{gx+}^{i,j,k}} \int\int \varphi_g(x_{i+1},y,z)\, dy\, dz - hk\, \varphi_g^{i,j,k}}{h/2} \right] \qquad (2.40)$$

The albedo used in QUANDRY is defined by

$$\int\int \varphi_g(x_{i+1},y,z)\, dy\, dz$$

$$= \alpha_{Q;g}^{i,j,k} \int\int J_{gx}(x_{i+1},y,z)\, dy\, dz \qquad (2.41)$$

The surface flux can be eliminated from these equations to yield for group g = 1, (neglecting the subscript),

$$L^{i,j,k\to i+1,j,k} = \left[\frac{h\, k}{\frac{h}{2D^{i,j,k}} + \frac{\alpha_Q^{i,j,k}}{f_{x+}^{i,j,k}}} \right] \varphi^{i,j,k} \qquad (2.42)$$

The corresponding expression in the FLARE model is

$$L^{i,j,k\to i',j',k'}$$

$$= \frac{1}{\lambda} S^{i,j,k} W^{i,j,k\to i',j',k'} (n^{i,j,k} - \alpha_F^{i,j,k}) \qquad (2.43)$$

where (i',j',k') represents the $n^{i,j,k}$ non-existent nodes adjacent to node (i,j,k), and $\alpha_F^{i,j,k}$ is the FLARE albedo. Following the FLARE approximation $W^{i,j,k\to i',j',k'}$ is replaced by $\tilde{W}^{i,j,k}$, and since we are treating each face separately $n^{i,j,k} = 1$, so that

$$L^{i,j,k\to i+1,j,k}$$

$$= \frac{1}{\lambda} \left[h^2 k \Sigma^{i,j,k} k_\infty^{i,j,k} \varphi^{i,j,k} \right] \tilde{W}^{i,j,k} (1 - \alpha_F^{i,j,k}) \qquad (2.44)$$

Equating the right-hand-sides of Equas. (2.42) and (2.44) yields

$$\alpha_F^{i,j,k} = 1 - \frac{\lambda}{h \Sigma_g^{i,j,k} k_\infty^{i,j,k} \tilde{W}^{i,j,k} \left[\frac{h}{2D^{i,j,k}} + \frac{\alpha_Q^{i,j,k}}{f_{x+}^{i,j,k}} \right]} \qquad (2.45)$$

In general,

$$\alpha^p_{F(u)} = 1 - \frac{\lambda}{\Delta u\ \Sigma^p\ k^p_\infty\ \tilde{W}^p \left[\frac{\Delta u}{2D^p} + \frac{\alpha^p_Q}{f^p_{u+}}\right]} \qquad (2.46)$$

$$u = x,y,z.$$

For a node on an edge or corner, which has two or three exterior surfaces, the "total albedo", of Equa. (2.37) is obtained by summing the contributions for each individual face.

We note that if $\alpha^p_Q = \infty$, (i.e. $\underline{n}\cdot\underline{J}_{sur} = 0$), then $\alpha^p_F = 1$; also if $\alpha^p_Q = 2$ (i.e. partial returning current $j- = 0$), and $\tilde{W}^p$ is replaced by the exact relation $W^{i,j,k\to i+1,j,k}$, then $\alpha^p_F = 0$, so that in this case the FLARE albedo represents the classical albedo $\alpha = [j-/j+]_{sur}$. When $W^{i,j,k\to i+1,j,k}$ is replaced by $\tilde{W}^{i,j,k}$, the FLARE albedo loses its physical character, and takes on the nature of a parameter, similar to the g-factor, which must be adjusted in order to obtain acceptable results.

It should be noted that the two approaches are consistent, since the sums of the contributions to the albedo α^p_F in the first case equal the total albedo $\alpha^p_{F(Tot)}$. The only reason for mentioning the first scheme is that it helps to decide how the averaging of the face-dependent g-factors should be carried out.

It has previously been noted that only the ratio α/f_{u+} appears in the QUANDRY-CMFD equations for the boundary nodes. Hence if average discontinuity factors $\tilde{f}_{in}$ are used, the albedo should be adjusted

using,

$$\alpha' = \frac{\bar{f}_{in}}{f_{u+}} \alpha \qquad (2.47)$$

so as to preserve the ratio α / f_{u+} . It should be noted, however, that Eq. (2.46) which relates the albedos in QUANDRY and FLARE contains the ratio α / f_{u+} explicitly. Hence it is not necessary to adjust the albedos, since the above ratio has been maintained.

SOLUTION OF FLARE EQUATIONS

A version of FLARE, which is called FLARE-G is available at MIT, and hence the FLARE equations can be solved using this code. The steps involved in the preparation of the FLARE data are listed as follows:

1. For a suitable bench-mark problem, two-group cross-sections $(D^{1,2}, \Sigma^{1,2}, \nu\Sigma_f^{1,2}, \ldots)$ are fixed. Two-group discontinuity factors $f_{u\pm}^{1,2}$ are obtained using assembly or color-set calculations. Two-group albedos are also required, and may be obtained from a fine-mesh solution or from a theoretical analysis.
2. The data in step 1 allows a two-group QUANDRY to be run using the quadratic approximation, which produces a solution that is taken to be the reference solution: eigenvalue λ ,two-group nodal fluxes and nodal powers, two-group surface fluxes and currents.

3. A one-group QUANDRY with the CMFD-approximation is then run using the restart option. This produces one-group collapsed cross-sections $D^1, \Sigma^1, \nu\Sigma^1, \ldots$; and one-group discontinuity factors $f^1_{u\pm}$ using the two-group nodal and surface fluxes in step 2. It was found that QUANDRY did not calculate one-group albedos for the restart problem; so this had to be corrected.

4. FLARE data can then be generated using a program NODPAR:

$$M_p^2 = \frac{D^p}{\Sigma^p} \; ; \qquad k_\infty^p = \frac{\nu\Sigma_f^p}{\Sigma^p}$$

$$g_{pq} = \frac{\dfrac{2\lambda}{(\Delta u)^2 \Sigma^p k_\infty^p}\left[\dfrac{f^p_{u\pm}}{\dfrac{f^p_{u\pm}}{D^p} + \dfrac{f^q_u}{D^q}}\right] - \dfrac{\sqrt{(M_p^2)}}{2(\Delta u)}}{\dfrac{M_p^2}{(\Delta u)^2} - \dfrac{\sqrt{(M_p^2)}}{2(\Delta u)}}$$

$$\alpha^p_{F(u)} = 1 - \frac{\lambda}{\Delta u \, \Sigma^p \, k_\infty^p \, \tilde{W}^p \left[\dfrac{\Delta u}{2D^p} + \dfrac{\alpha^p_Q}{f^p_{u+}}\right]}$$

$$u = x, y, z.$$

5. FLARE can be run in several options:

(a) Horizontal and vertical g's (g_h,g_v) and axially averaged albedos (standard FLARE)

(b) Node-dependent g's and axially averaged albedos

(c) Node-dependent g's and node-dependent albedos

FLARE RESULTS

Results were obtained using options (a) and (b) for a small benchmark problem EPRI-9 (3x3x4). The magnitude of the errors in all cases are consistent with those to be expected using the FLARE model. Figures (2-1) and (2-2) show the results obtained using g_h, g_v-values and node-dependent g-values respectively. For illustrative purposes, these figures also include results using QUANDRY but with the face-dependent discontinuity factors replaced by their node-averaged values. Since averaging discontinuity factors (or more precisely, the g-factors derived from the face-dependent discontinuity factors) is the only approximation made other than the axial averaging of the albedos, these should be much closer to the FLARE results, which is seen to be the case. It is to be noted that only a very small reduction in the relative errors of the eigenvalue λ and the assembly and mid-plane nodal power densities is achieved when node-dependent g-values are used. However, it was concluded that the small size of the core, with the majority of the nodes having external surfaces, did not make it a suitable test candidate for the FLARE model, with its inherent assumption that the kernel W^{pq} is the same for all adjacent nodes.

A more realistic test case is the SALEM-1 PWR (8x8x9). Results are shown in Figs. (2-3) and (2-4). It is immediately apparent that a very

dramatic improvement in the errors is obtained using node-dependent g-values. For example, the relative error in the eigenvalue decreased from - 0.34 % to - 0.11 %, and the maximum errors in the assembly power densities (in the interior of the core) from ≈ 15 % to ≈ 6%.

Depletion studies were carried out on ZION-2 (8x8x1). Results are shown in Figs. (2-5) - (2-10). As in the SALEM-1 case, there is a very significant reduction in the errors when node-dependent g-values are used, with the relative error in the eigenvalue decreasing from -0.26 % to -0.02 % at B-O-L. Maximum errors in the interior of the core are also reduced from ≈ 10 % to ≈ 4%. Both options show a large increase in the respective errors at the first depletion (60 hours), but these continue to increase more gradually up to the final depletion step (7800 hours). This result suggests that it would be preferable to use the 60-hour (equilibrium xenon) case to find the node-averaged discontinuity factors, thence g_p values.

EPRI-9: (3 x 3) x 4

ASSEMBLY POWER DENSITIES

EIGENVALUE (λ)

P_Q (Ref)	0.84908	0.63974	0.89255
P_Q ($\bar{f}$)	0.88433	0.69377	0.891070
P_F (g_H,g_V)	0.88555	0.69538	0.892093
Rel. Error (%)	4.30	8.70	-0.052
	1.1945	1.2827	
	1.1405	1.2907	
	1.14121	1.25273	
	-4.46	-2.34	
	1.3506		
	1.2722		
	1.30301		
	-3.52		

NODAL POWER DENSITIES

P_Q (Ref)	1.0656	0.80828	
P_Q ($\bar{f}$)	1.1193	0.88212	
P_F (g_H,g_V)	1.14203	0.89678	
Rel. Error (%)	7.17	10.95	
	1.5008	1.6293	
	1.4359	1.6387	
	1.47174	1.61556	
	-1.94	-0.84	
	1.6981		
	1.6015		
	1.68040		
	-1.04		

Fig. (2-1). Assembly and Mid-plane Nodal Power Densities Using (a) QUANDRY, (b) QUANDRY with $\bar{f}^P$, (c) FLARE-G with g_H, g_V.

EPRI-9: (3 x 3) x 4

ASSEMBLY POWER DENSITIES

			EIGENVALUE (λ)
P_Q (Ref)	0.84908	0.63974	0.892555
P_Q ($\bar{f}$)	0.88433	0.69377	0.891070
P_F (g_p)	0.88996	0.68800	0.892174
Rel. Error (%)	4.81	7.54	-0.043
	1.1945	1.2827	
	1.1405	1.2907	
	1.14449	1.28507	
	-4.19	0.18	
	1.3506		
	1.2722		
	1.27005		
	-5.96		

NODAL POWER DENSITIES

P_Q (Ref)	1.0656	0.80828	
P_Q ($\bar{f}$)	1.1193	0.88212	
P_F (g_p)	1.4697	0.87954	
Rel. Error (%)	7.64	8.82	
	1.5008	1.6293	
	1.4359	1.6387	
	1.46645	1.66607	
	-2.29	2.26	
	1.6981		
	1.6015		
	1.63206		
	-3.89		

Fig. (2-2). Assembly and Mid-plane Nodal Power Densities Using (a) QUANDRY, (b) QUANDRY with $\bar{f}^p$, (c) FLARE with g_p - values.

1.0718	P_Q (Ref)				
1.1751	P_F				
9.63	Rel. Error (%)				

0.9094	1.0819				
1.0506	1.1708				
15.53	8.22				

λ_Q (Ref) = 1.06521

λ_F = 1.06161

Rel. Error = -0.34%

1.0917	0.9133	1.0837			
1.1709	1.0401	1.1431			
7.25	13.89	5.48			

0.9418	1.1132	0.9059	1.0157		
1.0511	1.1603	0.9946	1.0449		
11.60	4.23	9.78	2.87		

1.1706	0.9714	1.1440	1.0047	1.1565	
1.1989	1.0516	1.1500	1.0398	1.0944	
2.42	8.26	0.52	3.49	-5.37	

1.0870	1.2041	0.9833	1.1554	0.9376	1.2214
1.1312	1.1828	1.0111	1.0935	0.8995	1.1232
4.07	-1.77	2.83	-5.36	-4.06	-8.04

1.1787	1.0616	1.1569	0.9709	0.9665	0.6301
1.1320	1.0552	1.0769	0.9580	0.8388	0.5783
-3.97	-0.60	-6.91	-1.33	-13.21	-8.22

0.8678	0.8565	0.9463	0.6661		
0.8508	0.8076	0.8636	0.5969		
-1.96	-5.71	-8.74	-10.38		

Fig. (2-3). Assembly Power Densities for SALEM-1 Using (a) QUANDRY, (b) FLARE-G with g_H, g_V.

1.0718	P_Q (Ref)				
1.1029	P_F				
2.90	Rel. Error (%)				

0.9094	1.0819				
0.8824	1.0929				
-2.97	1.01				

λ_Q = 1.06521

λ_F = 1.06640

Rel. Error = 0.11%

1.0917	0.9133	1.0837			
1.0999	0.8852	1.0720			
0.75	-3.08	-1.08			

0.9418	1.1132	0.9059	1.0152		
0.9007	1.0992	0.8636	0.9679		
-4.36	-1.26	-4.67	-4.70		

1.1706	0.9714	1.1440	1.0047	1.1565	
1.1577	0.9217	1.1152	0.9575	1.1164	
-1.10	-5.11	-2.52	-4.70	-3.47	

1.0870	1.2041	0.9833	1.1554	0.9376	1.2214
1.0284	1.1675	0.9261	1.1240	0.9015	1.3661
-5.39	-3.04	-5.82	-2.72	-3.85	11.85

1.1787	1.0616	1.1569	0.9709	0.9665	0.6301
1.1689	1.0189	1.1479	0.9873	1.0363	0.7175
-0.83	-4.02	-0.78	1.69	7.22	13.87

0.8678	0.8565	0.9463	0.6661		
0.9418	0.9171	1.0603	0.7442		
8.52	7.08	12.05	11.73		

Fig. (2-4). Assembly Power Densities for SALEM-1 Using (a) QUANDRY, (b) FLARE-G with g_p - Values.

0.9487	P_Q (Ref)				
1.0146	P_F				
6.95	Rel. Error (%)				

0.8431	0.9406				
0.9249	0.9884				
9.70	5.08				

λ_Q (Ref) = 1.00749

λ_F = 1.00488

Rel. Error = -0.26%

0.9717	0.8137	1.0082			
1.0163	0.8795	1.0395			
4.59	8.09	3.10			

0.9530	1.0682	0.9619	1.0971		
1.0244	1.1006	1.0172	1.0947		
7.49	3.03	5.75	-0.22		

1.1937	1.0501	1.1633	0.9509	1.2815	
1.2214	1.0953	1.1735	0.9769	1.2370	
2.32	4.30	0.88	2.73	-3.47	

1.2013	1.2484	1.1695	1.1666	0.8991	1.1419
1.2373	1.2504	1.1864	1.1322	0.8842	1.0750
3.00	0.16	1.45	-2.95	-1.66	-5.86

1.1742	1.0690	1.1389	1.0774	0.9316	0.5561
1.1372	1.0751	1.1038	1.0905	0.8869	0.4765
-3.15	0.57	-3.08	1.22	-4.80	-14.31

0.8625	0.9512	0.7945	0.6615		
0.8327	0.9035	0.7395	0.6120		
-3.46	-5.01	-6.92	-7.48		

Fig. (2-5). Nodal Power Densities for Zion-2 at B-O-L Using (a) QUANDRY, (b) FLARE-G with g_H, g_V.

0.9935	P_Q (Ref)				
1.1060	P_F				
11.32	Rel. Error (%)				

0.8657	0.9762				
0.9959	1.0670				
15.04	9.30				

λ_Q (Ref) = 1.00672

λ_F = 1.00339

Rel. Error = -0.33%

1.0023	0.8269	1.0285			
1.0859	0.9302	1.0922			
8.34	12.49	6.19			

0.9539	1.0844	0.9653	1.1062		
1.0629	1.1467	1.0439	1.1148		
11.43	5.75	8.14	0.78		

1.1962	1.0401	1.1632	0.9411	1.2866	
1.2481	1.1095	1.1883	0.9694	1.2050	
4.34	6.67	2.16	3.01	-6.34	

1.1695	1.2323	1.1496	1.1674	0.9074	1.1893
1.2308	1.2504	1.1738	1.1159	0.8527	1.0211
5.24	1.47	2.11	-4.41	-6.03	-14.14

1.1472	1.0277	1.1219	1.0667	0.9808	0.5936
1.1230	1.0469	1.0853	1.0511	0.8499	0.4566
-2.11	1.87	-3.26	-1.46	-13.35	-23.08

0.8252	0.9202	0.7837	0.6551
0.8086	0.8746	0.7196	0.5946
-2.01	-4.96	-8.18	-9.24

Fig. (2-6). Nodal Power Densities for Zion-2 at 60 Hrs. Using (a) QUANDRY, (b) FLARE-G with g_H, g_V.

1.2336	P_Q (Ref)				
1.3790	P_F				
11.79	Rel. Error (%)				
1.2193	1.2086				
1.4027	1.3486				
15.04	11.58				
1.2002	1.1443	1.1847			
1.3281	1.2977	1.2920			
10.66	13.41	9.06			
1.1859	1.1804	1.1826	1.1576		
1.3194	1.2732	1.2801	1.1876		
11.26	7.86	8.24	2.59		
1.1576	1.1621	1.1436	1.0792	1.1790	
1.2138	1.2365	1.1747	1.0757	1.0752	
4.85	6.40	2.72	-0.32	-8.80	
1.1440	1.0968	1.1331	1.0603	0.9444	0.9885
1.1694	1.1130	1.1289	1.0000	0.8143	0.8136
2.22	1.48	-0.37	-5.69	-13.78	-17.69
0.9724	0.9795	0.9521	0.9582	0.8304	0.5143
0.9615	0.9918	0.9201	0.9122	0.7046	0.3633
-1.12	1.26	-3.36	-4.80	-15.15	-29.36
0.6852	0.7474	0.6583	0.5624		
0.6495	0.7137	0.5795	0.4931		
-5.21	-4.51	-11.97	-12.32		

λ_Q(Ref) = 1.01314

λ_F = 1.00973

Rel. Error = -0.34%

Fig. (2-7). Nodal Power Densities for Zion-2 at 7800 Hrs. using (a) QUANDRY, (b) FLARE-G with g_H, g_V.

0.9487	P_Q (Ref)				
0.9620	P_F				
1.40	Rel. Error (%)				

$Q^{(Ref)}$ = 1.00749

Q_F = 1.00732

Rel. Error = -0.02%

0.8431	0.9406				
0.8278	0.9287				
-1.81	-1.27				
0.9717	0.8137	1.0082			
0.9610	0.7825	0.9768			
-1.10	-3.83	-3.11			
0.9530	1.0682	0.9619	1.0971		
0.9276	1.0403	0.9333	1.0500		
-2.67	-2.61	-2.97	-4.29		
1.1937	1.0501	1.1633	0.9509	1.2815	
1.1721	1.0093	1.1252	0.9123	1.2585	
-1.81	-3.89	-3.28	-4.06	-1.79	
1.2013	1.2484	1.1695	1.1666	0.8991	1.1419
1.1757	1.2198	1.1454	1.1370	0.8907	1.1872
-2.13	-2.29	-2.06	-2.54	-0.93	3.97
1.1742	1.0690	1.1389	1.0774	0.9316	0.5561
1.1670	1.0571	1.1396	1.1398	0.9940	0.5944
-0.61	-1.11	0.06	5.79	6.70	6.89
0.8625	0.9512	0.7945	0.6615		
0.9178	1.0389	0.8479	0.7225		
6.41	9.22	6.72	9.22		

Fig. (2-8). Nodal Power Densities for Zion-2 at B-O-L Using (a) QUANDRY, (b) FLARE-G with g_p- Values.

0.9935	P_Q (Ref)				
1.0695	P_F				
7.65	Rel. Error (%)				

0.8657	0.9762				
0.9045	1.0211				
4.48	4.60				

λ_Q(Ref) = 1.00672

λ_F = 1.00580

Rel. Error = -0.09%

1.0023	0.8269	1.0285			
1.0451	0.8381	1.0421			
4.27	1.35	1.32			

0.9539	1.0844	0.9653	1.1062		
0.9720	1.0993	0.9653	1.0799		
1.90	1.37	0.00	-2.38		

1.1962	1.0401	1.1632	0.9411	1.2866	
1.2104	1.0273	1.1491	0.9066	1.2213	
1.19	-1.23	-1.21	-3.67	-5.08	

1.1695	1.2323	1.1496	1.1674	0.9074	1.1893
1.1706	1.2270	1.1324	1.1233	0.8537	1.1126
0.09	-0.43	-1.50	-3.78	-5.92	-6.45

1.1472	1.0277	1.1219	1.0667	0.9808	0.5936
1.1558	1.0236	1.1224	1.0887	0.9433	0.5664
0.75	-0.40	0.04	2.06	-3.82	-4.58

0.8252	0.9202	0.7837	0.6551
0.8838	0.9962	0.8194	0.6997
7.10	8.26	4.56	6.81

Fig. (2-9). Nodal Power Densities for Zion-2 at 60 Hrs. Using (a) QUANDRY, (b) FLARE-G with g_p- Values.

1.2336	P_Q (Ref)				
1.2540	P_F				
1.65	Rel. (Error (%)				
1.2193	1.2086				
1.3609	1.2120				
11.61	0.28				
1.2002	1.1443	1.1847			
1.2025	1.2470	1.1620			
0.19	8.97	-1.92			
1.1859	1.1804	1.1826	1.1576		
1.3145	1.1617	1.2765	1.0848		
10.84	-1.58	7.94	-6.29		
1.1576	1.1621	1.1436	1.0792	1.1790	
1.1337	1.2637	1.0853	1.0772	0.9877	
-2.06	8.74	-5.10	-0.19	-16.23	
1.1440	1.0968	1.1331	1.0603	0.9444	0.9885
1.2039	1.0611	1.1669	0.9593	0.8556	0.8007
5.24	-3.25	2.98	-9.53	-9.40	-19.00
0.9724	0.9795	0.9521	0.9582	0.8304	0.5143
0.9725	1.0715	0.9332	0.9858	0.7394	0.4362
0.01	9.39	-1.99	2.88	-10.96	-15.19
0.6852	0.7474	0.6583	0.5624		
0.7239	0.7986	0.6761	0.5938		
5.65	6.85	2.70	5.58		

λ_Q(Ref) = 1.01314

λ_F = 1.01069

Rel. Error = -0.24%

Fig. (2-10). Nodal Power Densities for Zion-2 at 7800 Hrs. Using (a) QUANDRY, (b) FLARE-G with g_P- Values.

2.4 PRESTO MODEL: REDUCTION OF QUANDRY-CMFD EQUATIONS

We first approximate the six discontinuity factors for each node, $f_{gu\pm}^{i,j,k}$ $(u = x,y,z)$ by $\tilde{f}_g^{i,j,k}$, so that the QUANDRY-CMFD equations (2.26) become,

$$- 2k \left[\frac{\tilde{f}_g^{i+1,jk}}{D_g^{i+1,jk}} + \frac{\tilde{f}_g^{ijk}}{D_g^{ijk}} \right]^{-1} \left[\tilde{f}_g^{i+1,jk} \varphi_g^{i+1,jk} - \tilde{f}_g^{ijk} \varphi_g^{ijk} \right]$$

$$+ 2k \left[\frac{\tilde{f}_g^{i-1,jk}}{D_g^{i-1,jk}} + \frac{\tilde{f}_g^{ijk}}{D_g^{ijk}} \right]^{-1} \left[\tilde{f}_g^{ijk} \varphi_g^{ijk} - \tilde{f}_g^{i-1,jk} \varphi_g^{i-1,jk} \right]$$

$$- 2k \left[\frac{\tilde{f}_g^{i,j+1,k}}{D_g^{i,j+1,k}} + \frac{\tilde{f}_g^{ijk}}{D_g^{ijk}} \right]^{-1} \left[\tilde{f}_g^{i,j+1,k} \varphi_g^{i,j+1,k} - \tilde{f}_g^{ijk} \varphi_g^{ijk} \right]$$

$$+ 2k \left[\frac{\tilde{f}_g^{i,j-1,k}}{D_g^{i,j-1,k}} + \frac{\tilde{f}_g^{ijk}}{D_g^{ijk}} \right]^{-1} \left[\tilde{f}_g^{ijk} \varphi_g^{ijk} - \tilde{f}_g^{i,j-1,k} \varphi_g^{i,j-1,k} \right]$$

$$- \frac{2h^2}{k} \left[\frac{\tilde{f}_g^{ij,k+1}}{D_g^{ij,k+1}} + \frac{\tilde{f}_g^{ijk}}{D_g^{ijk}} \right]^{-1} \left[\tilde{f}_g^{ij,k+1} \varphi_g^{ij,k+1} - \tilde{f}_g^{ijk} \varphi_g^{ijk} \right]$$

$$+ \frac{2h^2}{k} \left[\frac{\tilde{f}_g^{ij,k-1}}{D_g^{ij,k-1}} + \frac{\tilde{f}_g^{ijk}}{D_g^{ijk}} \right]^{-1} \left[\tilde{f}_g^{ijk} \varphi_g^{ijk} - \tilde{f}_g^{ij,k-1} \varphi_g^{ij,k-1} \right]$$

$$+ h^2 k \, \Sigma_g^{i,j,k} \varphi_g^{i,j,k} = h^2 k \sum_{g'=1}^{G} \left[\frac{1}{\lambda} \chi_g \nu\Sigma_{fg'}^{i,j,k} + \Sigma_{gg'}^{i,j,k} \right] \varphi_{g'}^{i,j,k} \qquad (2.48)$$

We then define the following parameters:

$$\varphi_g^{*i,j,k} \equiv \tilde{f}_g^{i,j,k}\, \phi_g^{i,j,k}$$

$$D_g^{*i,j,k} \equiv \frac{D_g^{i,j,k}}{\tilde{f}_g^{i,j,k}}$$

$$\Sigma_g^{*i,j,k} \equiv \frac{\Sigma_g^{i,j,k}}{\tilde{f}_g^{i,j,k}} \tag{2.49}$$

so that

$$-2k \left[\frac{\tilde{f}_g^{i+1,jk}}{D_g^{i+1,jk}} + \frac{\tilde{f}_g^{ijk}}{D_g^{ijk}} \right]^{-1} \left[\tilde{f}_g^{i+1,jk} \varphi_g^{i+1,jk} - \tilde{f}_g^{ijk} \varphi_g^{ijk} \right]$$

$$= -2k \left[\frac{1}{D_g^{*i+1,j,k}} + \frac{1}{D_g^{*i,j,k}} \right]^{-1} \left[\varphi_g^{*i+1,j,k} - \varphi_g^{*i,j,k} \right]$$

$$= -2k \frac{D_g^{*i+1,j,k} \; D_g^{*i,j,k}}{D_g^{*i+1,j,k} + D_g^{*i,j,k}} \left[\varphi_g^{*i+1,j,k} - \varphi_g^{*i,j,k} \right] \tag{2.50}$$

and similarly for the other terms in Eq. (2.48). Hence the QUANDRY-CMFD equations are reduced to:

$$- \sum_{q_h=1}^{4} 2k \frac{D_g^{*p} D_g^{*q}}{D_g^{*p} + D_g^{*q}} \left[\varphi_g^{*q} - \varphi_g^{*p} \right] - \sum_{q_v=1}^{2} 2kR \frac{D_g^{*p} D_g^{*q}}{D_g^{*p} + D_g^{*q}} \left[\varphi_g^{*q} - \varphi_g^{*p} \right]$$

$$= h^2 k \sum_{g'=1}^{G} \left[\frac{1}{\lambda} \chi_g \nu \Sigma_{fg'}^{*p} + \Sigma_{gg'}^{*p} - \Sigma_{tg}^{*p} \delta_{gg'} \right] \varphi_{g'}^{*p} \qquad (2.51)$$

The fast group equation (g = 1) is given (neglecting the subscript) by :

$$- \sum_{q_h=1}^{4} 2k \frac{D^{*p} D^{*q}}{D^{*p} + D^{*q}} \left[\varphi^{*q} - \varphi^{*p} \right] - \sum_{q_v=1}^{2} 2kR \frac{D^{*p} D^{*q}}{D^{*p} + D^{*q}} \left[\varphi^{*q} - \varphi^{*p} \right]$$

$$= h^2 k \left[\frac{1}{\lambda} k_\infty^p - 1 \right] \Sigma^{*p} \varphi^{*p} \qquad (2.52)$$

This equation has the same structure as the PRESTO equation (2.20), except that only φ^{*p} occur here, whereas the previous equation contains φ^p and $\bar{\varphi}^p$. In order to make the form of the two equations identical, we rearrange the PRESTO equation by introducing the PRESTO expression for $\bar{\varphi}^p$ given by Eq. (2.14) into Eq. (2.20), which can finally be written as follows:

$$- \sum_{q_h=1}^{4} 2k \frac{D^p \; D^q}{D^p + D^q} \left[\varphi^q - \varphi^p \right] - \sum_{q_v=1}^{2} 2kR \frac{D^p \; D^q}{D^p + D^q} \left[\varphi^q - \varphi^p \right]$$

$$= h^2 k \left[\frac{1}{\lambda} k_\infty^p - 1 \right] \frac{\Sigma^p}{1+\gamma} \varphi^p \qquad (2.53)$$

where

$$\gamma_p = \frac{1}{2kD^p} \frac{(1 - a)/2}{3a + (1 - a)\ (R + 2)} h^2 k \left[\frac{1}{\lambda} k_\infty^p - 1 \right] \Sigma^p \qquad (2.54)$$

Except that D^p appears rather than D^{*p}, and center-point fluxes φ^p are replaced by fictitious nodal fluxes φ^{*p}, equation (2.53) is now identical to the reduced QUANDRY-CMFD equation (2.52), provided that we also interpret $\Sigma^p / (1+\gamma^p)$ as $\Sigma^{*p} = \Sigma^p / \tilde{f}^p$. This implies that

$$1 + \gamma^p = \tilde{f}^p$$

so that an expression for "a" may be determined from Eq. (2.54). It is given by:

$$a^p = \frac{h^2 \left[\frac{1}{\lambda} k_\infty^p - 1 \right] \Sigma^p - 4\ D^p\ (\tilde{f}^p - 1)\ (R + 2)}{h^2 \left[\frac{1}{\lambda} k_\infty^p - 1 \right] \Sigma^p + 4\ D^p\ (\tilde{f}^p - 1)\ (1 - R)} \qquad (2.55)$$

For R = 1, i.e. h = k:

$$a^p = 1 - \frac{12\, D^p\, (\bar{f}^p - 1)}{h^2 \left[\frac{1}{\lambda} k_\infty^p - 1 \right] \Sigma^p} \qquad (2.56)$$

SOLUTION OF PRESTO EQUATIONS

The PRESTO code is proprietary material, and hence is not available to the general public. Therefore, in order to test the above scheme, it is necessary to solve the PRESTO equations using some alternative code, which is available. Since QUANDRY was developed at MIT and is easily modified for the present purpose, it was decided that it could be used to solve the PRESTO equations. This is not completely satisfactory, and in fact appears a circular procedure, since QUANDRY is first used in order to determine the adjustable parameter a (or a^p). We take the view that the two stages are completely independent. In the first stage, by running QUANDRY in the normal manner, the parameters obtained, i.e. λ, $\bar{f}^p$,... etc. permit a^p to be calculated, and hence $a = \bar{a}^p$. Having determined "a", the PRESTO equations can now be solved by any suitable method, including of course PRESTO itself. It seems, however, that the different solutions thus obtained will not be identical, since different procedures, including the specification of boundary conditions are involved, and may not be exactly duplicated in each case. For example, it may be noted that an iterative scheme is used in PRESTO to solve the fast-group equation, which is written in an entirely equivalent form for the case h = k,

$$- \sum_{g=1}^{6} 2k \frac{D^p \; D^q}{D^p + D^q} \left[\varphi_1^q - \varphi_1^p \right]$$

$$= h^3 \left[\frac{1}{\lambda} \left[\frac{\nu\Sigma_{f1}^p}{\Sigma_1^p} + \frac{\nu\Sigma_{f2}^p \; \Sigma_{21}^p}{\Sigma_1^p \; \Sigma_2^p} F^p \right] - 1 \right] \Sigma_1^p \; \bar{\varphi}^p \qquad (2.57)$$

where $F^p = \bar{\bar{\varphi}}_2^p \; / \; \bar{\bar{\varphi}}_{2(asy)}^p$, $\bar{\bar{\varphi}}_2^p$ being the actual nodal-averaged thermal flux, and $\bar{\bar{\varphi}}_{2(asy)}^p$ the asymptotic value given by $\bar{\bar{\varphi}}_{2(asy)}^p = \left[\Sigma_{21}^p \; / \; \Sigma_2^p \right] \bar{\bar{\varphi}}_1^p$. F is initially set equal to unity, and the equation solved to yield $\bar{\bar{\varphi}}_1^p$, so that $\bar{\bar{\varphi}}_{2(asy)}^p$ can be determined. It is then assumed that the asymptotic values for the point fluxes φ_2^p hold at the centers of the nodes,

$$\varphi_2^p = \frac{\Sigma_{21}^p}{\Sigma_2^p} \bar{\bar{\varphi}}_1^p \qquad (2.58)$$

so that the thermal node-averaged flux may be reconstructed in a way similar to that used for the fast group,

$$\bar{\bar{\varphi}}_2^p \simeq a_2 \; \varphi_2^p + \frac{1 - a_2^p}{6} \sum_{q=1}^{6} \varphi_2^{pq} \qquad (2.59)$$

where a_2 is an adjustable parameter for the thermal group. The ratio

$F^p = \bar{\varphi}_2^p / \bar{\varphi}_{2(asy)}^p$ is then updated, so that the fast group can be solved again to obtain an improved value for $\bar{\varphi}_1^p$, and the iterative process repeated until convergence is achieved. A further approximation which we have neglected was introduced in PRESTO to reduce the data storage requirements.

In our case, however, the reference solution is already available, since it is necessary to determine the a_p-values. Thus we can use the known ratio of the thermal to fast flux to calculate $\bar{\varphi}_1^p$ directly (i.e. without iteration), and hence $\bar{\varphi}_2^p$ and the nodal powers. In particular, we note that when a = 1, the nodal volume-averaged fluxes $\bar{\varphi}^p$ and the centre-point fluxes φ^p are identical, and equations (2.52) and (2.53) are the same except that the "starred" cross-sections $(D^{*p}, \Sigma^{*p}, \ldots)$ given by Eq. (2.49) appear in place of the physical cross-sections $(D^p, \Sigma^p, \ldots)$. Hence, one approach to solving the PRESTO equations on QUANDRY is to set a = 1 and replace the physical cross-sections by their starred equivalents. While the flux solution obtained is a "fictitious nodal volume-averaged flux" φ^{*p}, the reaction rates are unchanged, so that the nodal powers have their true physical values, since

$$
\begin{aligned}
P^p &= \kappa \left[\Sigma_{f1}^{*p} \varphi_1^{*p} + \Sigma_{f2}^{*p} \varphi_2^{*p} \right] \\
&= \kappa \left[\frac{\Sigma_{f1}^p}{\bar{f}_1^p} \left[\bar{f}_1^p \varphi_1^p \right] + \frac{\Sigma_{f2}^p}{\bar{f}_2^p} \left[\bar{f}_2^p \varphi_2^p \right] \right] \\
&= \kappa \left[\Sigma_{f1}^p \varphi_1^p + \Sigma_{f2}^p \varphi_2^p \right] \qquad (2.60)
\end{aligned}
$$

One objection to this approach is that by setting a = 1, the fundamental assumption in the PRESTO model given by equations (2.14) and (2.15), which distinguishes the MCMFD model from previous CMFD models has been circumvented. However, there does not seem to be any alternative given the limitation of having to use QUANDRY to solve the PRESTO equations. In order to counter this objection, an investigation is currently being undertaken to use the nodal code SIMULATE with the PRESTO option, so that a direct comparison can be made between the two methods.

PRESTO RESULTS

Results were obtained using QUANDRY for the SALEM-1 pressurized water reactor at B-O-L, and are shown in Figs. (2-11) and (2-12). Since node-dependent discontinuity factors are used, this is equivalent to using PRESTO with node-dependent a_p-values . The relative error in the eigenvalue is < 0.2 %, with maximum errors of < 10 % in the assembly and nodal power densities. Depletion studies are presently being carried out on ZION - 2.

CONCLUSIONS

Until further testing is complete, conclusions must be tentative. However, at present, it appears that if node-dependent coupling coefficients and albedos are permitted for the FLARE and PRESTO models the accuracy is about that achieved when the usual trial-and-error procedure is used to find the adjustable parameters for the FLARE and SIMULATE models. There thus is no compelling reason to determine the FLARE and PRESTO parameters

1.0718	P_Q (Ref)				
1.1593	P_P				
8.16	Rel. Error (%)				
0.9094	1.0819				
0.9486	1.1214				
4.32	3.65				
1.0917	0.9133	1.0837			
1.1186	0.9592	1.1250			
2.46	5.03	3.81			
0.9418	1.1132	0.9059	1.0157		
0.9509	1.1309	0.9240	1.0173		
0.97	1.59	1.99	0.16		
1.1706	0.9714	1.1440	1.0047	1.1565	
1.1570	0.9875	1.1528	1.0097	1.1411	
-1.16	1.66	0.77	0.50	-1.33	
1.0870	1.2041	0.9833	1.1554	0.9376	1.2214
1.0540	1.1502	0.9708	1.0874	0.9119	1.2724
-3.04	-4.48	-1.26	-5.89	-2.74	4.18
1.1787	1.0616	1.1569	0.9709	0.9665	0.6301
1.1135	1.0194	1.0932	0.9673	0.9618	0.6603
-5.53	-3.98	-5.51	-0.38	-0.49	4.79
0.8678	0.8565	0.9463	0.6661		
0.8740	0.8858	0.9832	0.6777		
0.71	3.42	3.90	1.75		

$Q^{(Ref)}$ = 1.06521

P = 1.06336

Rel. Error = -0.17%

Fig. (2-11). Assembly Power Densities for SALEM-1 at B-O-L Using (a) QUANDRY, (b) PRESTO (QUANDRY).

1.6160	P_Q (Ref)				
1.7671	P_P				
9.35	Rel. Error (%)				
1.3709	1.6312				
1.4522	1.7197				
5.93	5.43				
1.6460	1.3768	1.6337			
1.7169	1.4699	1.7249			
4.31	6.76	5.58			
1.4197	1.6782	1.3656	1.5310		
1.4569	1.7340	1.4133	1.5496		
2.62	3.32	3.49	1.21		
1.7646	1.4642	1.7245	1.5143	1.7431	
1.7742	1.5116	1.7650	1.5414	1.7428	
0.54	3.24	2.35	1.79	-0.02	
1.6384	1.8150	1.4819	1.7414	1.4129	1.8402
1.6115	1.7593	1.4827	1.6591	1.3876	1.9317
-1.64	-3.07	0.05	-4.73	-1.79	4.97
1.7765	1.5997	1.7434	1.4630	1.4562	0.9493
1.7016	1.5553	1.6666	1.4696	1.4583	1.0014
-4.22	-2.78	-4.41	0.45	0.14	5.49
1.3076	1.2905	1.4257	1.0036		
1.3299	1.3430	1.4900	1.0054		
1.71	4.07	4.51	0.18		

Fig. (2-12). Mid-plane Nodal Power Densities for SALEM-1 at B-O-L Using (a) QUANDRY, (b) PRESTO (QUANDRY).

in this alternative manner, even though it is more systematic than the trial-and-error procedures in current use. In our opinion, computing effort required to implement the automatic scheme would be far better spent on a production version of QUANDRY.

3. DEVELOPMENT OF A MORE EFFICIENT FLUX RECONSTRUCTION METHOD FOR BWRs - A. Z. TANKER

Although discontinuity factors found from assembly calculations lead to accurate predictions of k_{eff} and average nodal powers for BWRs, reconstructing detailed pin power shapes has required the use of response matrices or extended assembly calculations.

During the past year, computer codes have been constructed to carry out the reconstruction using a fine-mesh, beginning-of-life, quarter-core solution. A small, "benchmark," test problem has been created and a one-cycle depletion carried out. We are now applying our new flux-reconstruction method to this reference case and expect to complete the testing during the coming year.

4. Development of Methods to Analyze Transients - Antonio Dias

We had hoped, during the past year, to begin an investigation of the use of "supernodes" (of size $\approx$ 40 x 40 x 60 cm^3) for the analysis of reactor transients. However, the static application of this technique (supported by other funds) ran into a technical difficulty which we are only now beginning to understand. That understanding does, however, indicate that applying the method to transient analysis is still an attractive possibility. We hope to explore it during the coming year.

For many situations, however, transients that occur in a reactor have a one-dimensional character such that the perturbations are uniform in radial planes but quite non-uniform in the axial direction. Examples of such transients are a rod bank withdrawal, a loss of flow accident and a turbine trip accident. The assumption that the x,y shape of the neutron distribution is unperturbed during the transient is then more plausible than that required for the point kinetics approach. Introducing this idea into a nodal method should result in a theory that allows the simulation of certain transients with better precision than if point kinetics were used, but with greater speed than if a full 3-D nodal approach were considered.

A one-dimensional model is available on option in the RETRAN code. However, it appears to ignore radial leakage effects. In the work described below, we have used a variational principle to derive one-dimensional, G-group transient equations directly from the QUANDRY nodal equations. This procedure has the advantage of treating radial leakage effects in a theoretically consistent way. In addition, the parameters needed for the one-dimensional equations can be computed directly from a static, three-dimensional, beginning-of-transient QUANDRY solution. Of even greater utility is the fact that it will be possible to test the accuracy of the

one-dimensional equations by direct comparison with three-dimensional QUANDRY results based on consistent time-dependent nodal cross sections.

4.1 Derivation of the Theory

The QUANDRY nodal equations for a 3-D transient problem can be represented as:[1]

$$\begin{bmatrix} [V^{-1}] & [o] & [o] & [o] & [o] & \cdots & [o] \\ [o] & [o] & [o] & [o] & [o] & \cdots & [o] \\ [o] & [o] & [o] & [o] & [o] & \cdots & [o] \\ [o] & [o] & [o] & [o] & [o] & \cdots & [o] \\ [o] & [o] & [o] & [o] & [o] & \cdots & [o] \\ \vdots & \vdots & \vdots & \vdots & \vdots & \ddots & \vdots \\ [o] & [o] & [o] & [o] & [o] & \cdots & [o] \end{bmatrix} \frac{d}{dt} \begin{bmatrix} [\bar{\phi}(t)] \\ [\bar{L}_x(t)] \\ [\bar{L}_y(t)] \\ [\bar{L}_z(t)] \\ [\bar{C}_1(t)] \\ \vdots \\ [\bar{C}_D(t)] \end{bmatrix} =$$

$$= \begin{bmatrix} [M_p(t)]-[\Sigma_T(t)] & -h_y^j h_z^k[I] & -h_x^i h_z^k[I] & -h_x^i h_y^j[I] & \lambda_1[I] & \cdots & \lambda_D[I] \\ [F_x(t)] & -[I] & \frac{1}{h_y^j}[G_x(t)] & \frac{1}{h_z^k}[G_x(t)] & [o] & \cdots & [o] \\ [F_y(t)] & \frac{1}{h_x^i}[G_y(t)] & -[I] & \frac{1}{h_z^k}[G_y(t)] & [o] & \cdots & [o] \\ [F_z(t)] & \frac{1}{h_x^i}[G_z(t)] & \frac{1}{h_y^j}[G_z(t)] & -[I] & [o] & \cdots & [o] \\ [M_1(t)] & [o] & [o] & [o] & -\lambda_1[I] & \cdots & [o] \\ \vdots & \vdots & \vdots & \vdots & \vdots & \ddots & \vdots \\ [M_D(t)] & [o] & [o] & [o] & [o] & \cdots & -\lambda_D[o] \end{bmatrix} \begin{bmatrix} [\bar{\phi}(t)] \\ [\bar{L}_x(t)] \\ [\bar{L}_y(t)] \\ [\bar{L}_z(t)] \\ [\bar{C}_1(t)] \\ \vdots \\ [\bar{C}_D(t)] \end{bmatrix} \quad (4.1)$$

where:

$[\bar{\phi}(t)]$ ≡ a column vector of length G x (I x J x K) (≡N) containing the node averaged fluxes (ordered first by group, then x-direction, then y-direction, and finally z-direction)

$[\bar{L}_u(t)]$ ≡ a column vector of length N containing the u-directed net leakages for each node • u = x, y, or z

$[\bar{C}_d(t)]$ ≡ a column vector of length N containing, for the d-precursor family, the elements of $V_{ijk}[\chi_d]\bar{C}_{d_{ijk}}(t)$

$[V^{-1}]$ ≡ a block diagonal matrix of order N x N containing the elements of $V_{ijk}[v]^{-1}$

$[M_p(t)]$ ≡ a block diagonal matrix of order N x N containing the elements of $(1-\beta)V_{ijk}[\chi_p]\ [\nu\Sigma_{f_{ijk}}(t)]^T$

$[\Sigma_T(t)]$ ≡ a block diagonal matrix of order N x N containing the elements of $V_{ijk}[\Sigma_{T_{ijk}}(t)]$ with $[\Sigma_{T_{ijk}}(t)]$ equal to the G x G matrix $\{\delta_{gg'}\Sigma^{(ijk)}_{tg} - \Sigma^{(ijk)}_{gg'}\}$

$[F_u(t)]$ ≡ a block tridiagonal matrix of order N x N containing the elements of $[F^{\ell}_{u_{\ell mn}}(t)]$ specifying leakage in the u-direction

$[G_u(t)]$ ≡ a block pentadiagonal matrix of order N x N containing the elements of $[G^{\ell}_{u_{\ell mn}}(t)]$ specifying leakage transverse to the u-direction

$[M_d(t)]$ ≡ a block diagonal matrix of order N x N containing, for the d-precursor family, the elements of $\beta_d V_{ijk}[\chi_d]\ [\nu\Sigma_{f_{ijk}}(t)]^T$

Detailed expressions for the elements of the vectors and matrices cited above are given in Reference (8).

The systematic derivation of equations presented in this work is due to the application of a synthesis method based on a variational principal (3),(9). In order to implement this approach, it is necessary to construct a functional that is made stationary by the solutions of the QUANDRY equations (eq. 4.1).

The functional in question is defined for a set of functions:

$$\{[u(t)], [v_x(t)], [v_y(t)], [v_z(t)], [c_1(t)], \ldots, [c_D(t)], [u^*(t)],$$
$$[v_x^*(t)], [v_y^*(t)], [v_z^*(t)], [c_1^*(t)], \ldots, [c_d^*(t)]\}$$

these functions are to be continuous in time within the time interval (t_o, t_f), during which the simulation takes place.

Each of these functions is actually a column vector of length G·I·J·K

The expression for the functional is:

$$F([u], [v_x], [v_y] \; [v_z] \; [c_1], \ldots, [c_D], [u^*], [v_x^*], [v_y^*], [v_z^*], [c_1^*], \ldots,$$
$$[c_D^*]) = \int_{to}^{t_f} dt \{ [\,[u^*]\,[v_x^*]\,[v_y^*]\,[v_z^*]\,[c_1^*] \ldots [c_D^*]\,]^T \quad x$$

$$
\begin{bmatrix}
[M_p]-[\Sigma_T]-[V^{-1}]\frac{d}{dt} & -h_y^j h_z^k[I] & -h_x^i h_z^k[I] & -h_x^i h_y^j[I] & \lambda_1[I] \ldots \lambda_D[I] \\
[F_x] & -[I] & \frac{1}{h_y^j}[G_x] & \frac{1}{h_z^k}[G_x] & [O] \ldots [O] \\
[F_y] & \frac{1}{h_x^i}[G_y] & -[I] & \frac{1}{h_z^k}[G_y] & [O] \ldots [O] \\
[F_z] & \frac{1}{h_x^i}[G_z] & \frac{1}{h_y^j}[G_z] & -[I] & [O] \ldots [O] \\
[M_1] & [O] & [O] & [O] & -\frac{d}{dt}-\lambda_1 \quad [O] \\
\vdots & \vdots & \vdots & \vdots & \ddots \\
[M_1] & [O] & [O] & [O] & [O] \ldots -\frac{d}{dt}-\lambda_D[I]
\end{bmatrix}
\begin{bmatrix} [u] \\ [v_x] \\ [v_y] \\ [v_z] \\ [c_1] \\ \vdots \\ [c_D] \end{bmatrix} \quad (4.2)
$$

where $\frac{d}{dt}$ is considered as an operator.

In order to keep notation simpler, the time-dependence is not shown. Such suppression will be adopted for all equations which follow.

For the application of the synthesis method, the following set of trial functions are defined:

$$
\begin{aligned}
[u] &= [\bar{\psi}]\,[T] & [u^*] &= [\bar{\psi}^*]\,[T^*] \\
[v_x] &= [\bar{\xi}]\,[X] & [v_x^*] &= [\bar{\xi}^*]\,[X^*] \\
[v_y] &= [\bar{\eta}]\,[Y] & [v_y^*] &= [\bar{\eta}^*]\,[Y^*] \\
[v_z] &= [\bar{\zeta}]\,[Z] & [v_z^*] &= [\bar{\zeta}^*]\,[Z^*] \\
[c_1] &= [\bar{c}_1] & [c_1^*] &= [\bar{c}_1^*] \\
&\vdots & &\vdots \\
[c_D] & [\bar{c}_D] & [c_D^*] &= [\bar{c}_D^*]
\end{aligned} \quad (4.3)
$$

where $[\bar{\psi}]$, $[\bar{\xi}]$, $[\bar{\eta}]$, $[\bar{\zeta}]$ are matrices constructed from the vectors $[\bar{\phi}]$, $[\bar{L}_x]$, $[\bar{L}_y]$, $[\bar{L}_z]$ obtained from a QUANDRY run for the steady state situation existing just before the transient to be simulated. Those matrices all have the same structure. For example:

$$[\bar{\psi}] = \begin{bmatrix} \bar{\phi}_{111} & 0 & 0 \cdots \\ \bar{\phi}_{211} & 0 & 0 \cdots \\ \bar{\phi}_{311} & 0 & 0 \cdots \\ \vdots & \vdots & \vdots \\ \bar{\phi}_{IJ1} & 0 & 0 \cdots \\ 0 & \bar{\phi}_{112} & 0 \cdots \\ 0 & \bar{\phi}_{212} & 0 \cdots \\ \vdots & \vdots & \vdots \end{bmatrix}$$

where: $\bar{\phi}_{ijk} = \begin{bmatrix} \bar{\phi}_{1ijk} & 0 & \cdots & 0 \\ 0 & \bar{\phi}_{2ijk} & \cdots & 0 \\ \vdots & \vdots & \ddots & \vdots \\ 0 & 0 & \cdots & \bar{\phi}_{Gijk} \end{bmatrix}$ G being the number of energy groups

$[\bar{\psi}]$ is thus a $G \cdot I \cdot J \cdot K \times G \cdot K$ matrix

The weight functions $[\bar{\psi}^*]$, $[\bar{\xi}^*]$, $[\bar{\eta}^*]$, $[\bar{\zeta}^*]$ have the same structure but contain elements obtained from a steady-state adjoint QUANDRY run (or some reasonable approximation thereto).

$[T]$, $[X]$, $[Y]$, $[Z]$, $[T^*]$, $[X^*]$, $[Y^*]$, $[Z^*]$ are the unknown vectors that specify the time-dependent axial behavior of the solution. They all have the same structure. For example:

$$[T] = \begin{bmatrix} T_1 \\ T_2 \\ \vdots \\ T_k \end{bmatrix}$$

where: $T_k = \begin{bmatrix} T_{1k} \\ T_{2k} \\ \vdots \\ T_{Gk} \end{bmatrix}$ G being the number of energy groups

As will be seen below, there is no need to approximate the precursor concentration vectors $[\bar{c}_d(t)]$ defined in connection with Eq. (4.1). Thus the $[c_d]$ in (4.2) are taken as the $[\bar{c}_d]$ themselves.

Note that $[u] = [\bar{\psi}]\,[T]$, and all the other trial functions, are column vectors of length $G \cdot I \cdot J \cdot K$ $(\equiv N)$ as required by Eq. (4.2).

The synthesis approximation is to assume that the x,y shape of the neutron population of each axial layer is unchanged, during the transient, from the steady state QUANDRY run that generated it. The transient problem is then simulated as a fixed x,y nodal shape for nodal fluxes and net leakages, in the k-th layer of the reactor, multiplied by the time-dependent factors $T_k(t)$, $X_k(t)$, $Y_k(t)$, $Z_k(t)$.

If the trial functions of Eqs. (4.3) are inserted into the functional of Eq. (4.2), and the variations of the functional with respect to $[T^*]$, $[X^*]$, $[Y^*]$, $[Z^*]$, and the $[\bar{c}_d^*]$ are set successively to zero, the following equations result:

$$[\bar{\psi}^*]^T [V^{-1}] \frac{d}{dt} [\bar{\psi}]\,[T] = [\bar{\psi}^*]^T [M_p]\,[\bar{\psi}]\,[T] - [\bar{\psi}^*]^T [\Sigma_T]\,[\bar{\psi}]\,[T] -$$
$$- h_y^j h_z^k\, [\bar{\psi}^*]^T [\bar{\xi}]\,[X] - h_x^i h_z^k\, [\bar{\psi}^*]^T [\bar{\eta}]\,[Y] -$$
$$- h_x^i h_y^j\, [\bar{\psi}^*]^T [\bar{\zeta}]\,[Z] + \sum_{d=1}^{D} \lambda_d\, [\bar{\psi}^*]^T [\bar{c}_d]$$

$$[\bar{\xi}^*]^T [F_x]\,[\bar{\psi}]\,[T] - [\bar{\xi}^*]^T [\bar{\xi}]\,[X] + \frac{1}{h_y^j}\, [\bar{\xi}^*]^T [G_x]\,[\bar{\eta}]\,[Y] +$$
$$+ \frac{1}{h_z^k}\, [\bar{\xi}^*]^T [G_x]\,[\bar{\zeta}]\,[Z] = 0$$

$$[\bar{\eta}^*]^T [F_y] [\bar{\psi}] [T] + \frac{1}{h_x^i} [\bar{\eta}^*]^T [G_y] [\bar{\xi}] [X] - [\bar{\eta}^*]^T [\bar{\eta}] [Y] +$$

$$+ \frac{1}{h_z^k} [\bar{\eta}^*]^T [G_y] [\bar{\zeta}] [Z] = 0$$

$$[\bar{\zeta}^*]^T [F_z] [\bar{\psi}] [T] + \frac{1}{h_x^i} [\bar{\zeta}^*]^T [G_z] [\bar{\xi}] [X] + \frac{1}{h_y^j} [\bar{\zeta}^*]^T [G_z] [\bar{\eta}] [Y] -$$

$$- [\bar{\zeta}^*]^T [\bar{\zeta}] [Z] = 0$$

$$\frac{d}{dt} [\bar{C}_d] = [M_d] [\bar{\psi}] [T] - \lambda_d [\bar{C}_d] \qquad d = 1, \ldots, D$$

These equations can be written in a more simplified way as:

$$[AA0] \frac{d}{dt} [T] = ([AA2p] - [AA1]) [T] - [AA3] [X] - [AA4] [Y] - [AA5] [Z] +$$

$$+ \sum_{d=1}^{D} \lambda_d [\bar{\psi}^*]^T [\bar{C}_d] \tag{4.4}$$

$$[BB1] [T] - [BB2] [X] + [BB3] [Y] + [BB4] [Z] = 0 \tag{4.5}$$

$$[CC1] [T] + [CC2] [X] - [CC3] [Y] + [CC4] [Z] = 0 \tag{4.6}$$

$$[DD1] [T] + [DD2] [X] + [DD3] [Y] - [DD4] [Z] = 0 \tag{4.7}$$

$$\frac{d}{dt} [\bar{C}_d] = [M_d] [\bar{\psi}] [T] - \lambda_d [\bar{C}_d] \qquad d = 1, \ldots, D \tag{4.8}$$

The definition of each new matrix can be found by comparing the two sets of equations.

Because of the non-square structure of the weighting matrices, $[\bar{\psi}^*]^T$, $[\bar{\eta}^*]^T$, etc., and expansion functions $[\bar{\psi}]$, $[\bar{\eta}]$, etc., the matrices in (4.4) - (4.7) are only of order G•K x G•K. In fact, many have very simple forms. Specifically, [AA0], [AA1], [AA2p], [AA3], [AA4], [AA5], [BB1], [BB2], [BB3],

[BB4], [CC1], [CC2], [CC3], [CC4], [DD4] are block diagonal matrices of order G•K x G•K, [DD1] is a block tridiagonal matrix of order G•K x G•K and [DD2], [DD3] are block pentadiagonal matrices of order G•K x G•K

The fact that so many of these matrices are block diagonal eases considerably the process of solving the set of Eqs. (4.4) - (4.8). Thus, from Eqs. (4.5) and (4.6) we find:

$$[X] = [EE1]\,[T] + [EE2]\,[Z] \tag{4.9}$$

$$[Y] = [FF1]\,[T] \quad [FF2]\,[Z] \tag{4.10}$$

where: $[EE1] \equiv \{[CC3]\,[BB3]^{-1}\,[BB2] - [CC2]\}^{-1}\,\{[CC3]\,[BB3]^{-1}\,[BB1] + [CC1]\}$

$[EE2] \equiv \{[CC3]\,[BB3]^{-1}\,[BB2] - [CC2]\}^{-1}\,\{[CC3]\,[BB3]^{-1}\,[BB4] + [CC4]\}$

$[FF1] \equiv \{[BB2]\,[CC2]^{-1}\,[CC3] - [BB3]\}^{-1}\,\{[BB2]\,[CC2]^{-1}\,[CC1] + [BB1]\}$

$[FF2] \equiv \{[BB2]\,[CC2]^{-1}\,[CC3] - [BB3]\}^{-1}\,\{[BB2]\,[CC2]^{-1}\,[CC4] + [BB4]\}$

The matrices [EE1], [EE2], [FF1], [FF2] are block diagonal of order G•K• x G•K

Substituting Eqs. (4.9) and (4.10) into Eqs. (4.4) and (4.7) we find:

$$[AA0]\,\frac{d}{dt}\,[T] = [HH1]\,[T] - [HH2]\,[Z] + \sum_{d=1}^{D} \lambda_d\,[\bar{\psi}^*]^T\,[\bar{c}_d] \tag{4.11}$$

$$[II1]\,[T] - [II2]\,[Z] = 0 \tag{4.12}$$

where: $[GG] \equiv [AA2p] - [AA1]$

$[HH1] \equiv [GG] - [AA3]\,[EE1] - [AA4]\,[FF1]$

$[HH2] \equiv [AA3]\,[EE2] + [AA4]\,[FF2] + [AA5]$

$[II1] \equiv [DD1] + [DD2]\,[EE1] + [DD3]\,[FF1]$

$[II2] \equiv [DD4] - [DD2]\,[EE2] - [DD3]\,[FF2]$

[GG], [HH1], [HH2] are block diagonal matrices of order G·K x G·K

[II1], [II2] are block pentadiagonal matrices of order G K x G K

Multiplying Eq. (4.11) by $[II2]\,[HH2]^{-1}$ and using Eq. (4.12) we can write:

$$[KK]\,\frac{d}{dt}\,[T] = [LL]\,[T] + [JJ]\sum_{d=1}^{D}\lambda_d\,[\bar{\psi}^*]^T\,[\bar{C}_d] \tag{4.13}$$

where: $[JJ] \equiv [II2]\,[HH2]^{-1}$

$[KK] \equiv [JJ]\,[AA0]$

$[LL] \equiv [JJ]\,[HH1] - [II1]$

[JJ], [KK], [LL] are block pentadiagonal matrices of order G·K x G·K

Multiplying Eqs. (4.8) by $[\psi^*]^T$ we can write a more simplified set of equations than Eqs. (4.8) and (4.13):

$$[KK]\,\frac{d}{dt}\,[T] = [LL]\,[T] + [JJ]\sum_{d=1}^{D}\lambda_d\,[P_d] \tag{4.14}$$

$$\frac{d}{dt}\,[P_d] = [MM_d]\,[T] - \lambda_d\,[P_d] \qquad d = 1, \ldots, D \tag{4.15}$$

where: $[P_d] \equiv [\bar{\psi}^*]^T\,[\bar{C}_d]$

$[MM_d] \equiv [\bar{\psi}^*]^T\,[M_d]\,[\bar{\psi}]$

$[P_d]$ are block vectors of length G·K

$[MM_d]$ are block diagonal matrices of order G·K x G·K

Following the same method used by QUANDRY for solving the transient equations, Eq. (4.15) is analytically solved assuming a linear behavior for $[MM_d]$ and $[T]$ during a time step. With that assumption, one can find an expression for $[P_d^{n+1}] \equiv [P_d(t^{n+1})]$ which can now be substituted into

Eq. (4.14), when that equation is solved numerically by the application of the θ-method. The resultant equations can be written as:

$$[UU]\,[T^{n+1}] = [U] \tag{4.16}$$

$$[P_d^{n+1}] = X_d\,[P_d^{n}] + \frac{1}{\lambda_d}\,\{[NN_d]\,[T^{n+1}] + [QQ_d]\,[T^{n}]\} \qquad d = 1, \ldots, D \tag{4.17}$$

where: $[UU] \equiv [SS] - \Delta_n \theta\,[LL^{n+1}]$

$[SS] \equiv [JJ^{n+1}]\,[RR]$

$$[RR] \equiv [AAO] - \Delta_n \theta \sum_{d=1}^{D} [NN_d]$$

$$[NN_d] \equiv f_1(\lambda_d\Delta_n)\,[MM_d^{n+1}] + f_2(\lambda_d\Delta_n)\,[MM_d^{n}]$$

$$[QQ_d] \equiv f_2(\lambda_d\Delta_n)\,[MM_d^{n+1}] + f_3(\lambda_d\Delta_n)\,[MM_d^{n}]$$

$$[Q_d] = [QQ_d]\,[T^n]$$

$$\Delta_n \equiv (t^{n+1} - t^n)$$

$$X_d = e^{-\lambda_d\Delta_n}$$

$$f_1(\lambda_d\Delta_n) = \begin{cases} 1 - \dfrac{2}{\lambda_d\Delta_n} + 2.\dfrac{1-X_d}{(\lambda_d\Delta_n)^2} & ;\ \text{if } \lambda_d\Delta_n > 0.1 \\ \dfrac{\lambda_d\Delta_n}{3}\left[1 - \dfrac{\lambda_d\Delta_n}{4}\left[1 - \dfrac{\lambda_d\Delta_n}{5}\left[1 - \dfrac{\lambda_d\Delta_n}{6}\right]\right]\right] & ;\ \text{if } \lambda_d\Delta_n \le 0.1 \end{cases}$$

$$f_2(\lambda_d\Delta_n) = \begin{cases} \dfrac{1+X_d}{\lambda_d\Delta_n} - 2.\dfrac{1-X_d}{(\lambda_d\Delta_n)^2} & ;\ \text{if } \lambda_d\Delta_n > 0.1 \\ \dfrac{\lambda_d\Delta_n}{2}\left[\dfrac{1}{3} - \dfrac{\lambda_d\Delta_n}{2}\left[\dfrac{1}{3} - \dfrac{\lambda_d\Delta_n}{5}\left[\dfrac{1}{2} - \dfrac{\lambda_d\Delta_n}{9}\right]\right]\right] & ;\ \text{if } \lambda_d\Delta_n \le 0.1 \end{cases}$$

$$f_3(\lambda_d\Delta_n) = \begin{cases} -X_d - \dfrac{2\,X_d}{\lambda_d\Delta_n} + 2.\dfrac{1-X_d}{(\lambda_d\Delta_n)^2} & ;\ \text{if } \lambda_d\Delta_n > 0.1 \\ \lambda_d\Delta_n \left(\dfrac{1}{3} - \dfrac{\lambda_d\Delta_n}{2}\left(\dfrac{1}{2} - \lambda_d\Delta_n\left(\dfrac{1}{5} - \dfrac{\lambda_d\Delta_n}{18}\right)\right)\right) & ;\ \text{if } \lambda_d\Delta_n < 0.1 \end{cases}$$

$$[U] \equiv [JJ^{n+1}]\,[S]$$

$$[S] \equiv [R1] + \Delta_n\left((1-\theta)\,[R2^n] + \theta[R3] + [R4]\right)$$

$$[R1] \equiv [AA0]\,[T^n]$$

$$[R2^n] \equiv [JJ^n]^{-1}\,[LL^n]\,[T^n] \qquad (4.18)$$

$$[R3] \equiv \sum_{d=1}^{D} [Q_d]$$

$$[R4] \equiv \sum_{d=1}^{D} \lambda_d\left(1 - \theta(1-X_d)\right)\,[P_d^n]$$

$[NN_d]$, $[QQ_d]$, $[RR]$ are block diagonal matrices of order G·K x G·K

$[SS]$, $[UU]$ are block pentadiagonal matrices of order G·K x G·K

$[Q_d]$, $[R1]$, $[R2^n]$, $[R3]$, $[R4]$, $[S]$, $[U]$ are block vectors of length G·K

The matrix $[UU]$ multiplying $[T^{n+1}]$ in (4.16) is block pentadiagonal, and the vector $[U]$ contains a term $[R1^n]$ which involves the inverse of the block pentadiagonal matrix $[JJ^n]$. Thus to find $[U]$ and then $[T^{n+1}]$, two linear systems have to be solved for each time step calculation. Because the matrix of coefficients in both cases is compact around the main diagonal, the application of an elimination procedure, instead of a more complex iterative one, for solving the systems is acceptable.

In order to calculate the coupling matrices $[F_u]$, $[G_u]$ $u = x, y, z$ during the transient, the following expressions are used for estimating the frequencies representing the time variation of the nodal fluxes and the precursors concentrations:

$$\omega^n_{p_{gijk}} = \omega^n_{p_{gk}} = \frac{1}{\Delta_{n-1}} \ell n \left(\frac{T^n_{gk}}{T^{n-1}_{gk}} \right) \tag{4.19}$$

$$\omega^n_{d_{ijk}} = \omega^n_{d_k} = \frac{1}{\Delta_{n-1}} \ell n \left(\frac{\sum_{g=1}^{G} P^n_{d_{gk}}}{\sum_{g=1}^{G} P^{n-1}_{d_{gk}}} \right) \tag{4.20}$$

Note that those values are to be applied to all nodes in a given plane.

4.2 Computational Implementation

The matrices defined for the numerical solution of the transient equations are, at most, block pentadiagonal, and a lot of memory would be required to store their null terms if the full matrices were stored. A special storage scheme where only the diagonal terms are preserved is thus appropriate in order to lower the amount of memory needed for the code representing the theory here developed.

Another observation is that many of the matrices are only temporary results used in the process of finding the solutions $[T^{n+1}]$ and $[P_d{}^{n+1}]$ for a given time step. A procedure such as dynamic allocation, in which a certain area of memory is commonly used by the program to store temporarily needed results, is thus an appealing approach towards improving calculational efficiency.

The combination of these two special computational strategies is expected to make the code faster and less memory-demanding than if a standard matricial representation were used.

4.3 Present Status and Future Work

Because some of the software necessary for manipulating the matrices is being handled by the code itself in order to provide the economy of memory cited above, special care was needed in the construction and implementation of the code. There were many intermediary testing stages before the whole theory was put together. At the moment this has been done, and basic tests, such as transients with $\Delta_n = 0$ or "transients" where actually nothing happens are being performed for very simple reactor configurations. These tests constitute a check of the precision and stability of the method being used.

The next step in the implementation of the theory will be to simulate transient conditions by the variation of the composition of certain nodes. For many cases, comparisons can be made with results obtained from other computer codes using a different methodology for the problem.

A step further will be the inclusion of a simple thermal-hydraulic model such as the one used by QUANDRY, in order to represent feedback effects.

5. Time Integration Schemes For The Point Kinetics Equations - Alex Parlos

The running time of computer codes which solve neutron transient problems is usually directly proportional to the number of time steps required to cover the time duration of interest. Thus, any calculational method that allows a decrease in the number of time steps (or, equivalently, an increase in the size of the time step) will decrease the cost of a transient calculation. Such savings will be most important for long-running, spatially dependent transients. However, methods developed for the space-independent, point kinetics model are still of interest since they may be extendable to space-dependent calculations and since a fast solution of the point kinetics equations will permit prediction of transient behavior in faster than real time, a capability that permits consideration of new advanced control and safety procedures.

5.1 Theory

The mathematical feature that leads to the need for short time steps in the numerical solution of transient equations is the fact that some of the time constants involved in the calculations are very short, while others are very long. The equations are said to be "stiff".

The basic idea in the formulation and solution of the space independent kinetics model comes from reference (10). It is the simple observation that the stiffness characteristic is present only in the time response of the prompt neutron density but not in that of delayed neutron precursors. With the usual notation, the point kinetics equations may be written:

$$\frac{dN(t)}{dt} = \frac{\rho(t)-\beta}{\Lambda} N(t) + \sum_{i=1}^{I} \lambda_i C_i(t) \tag{5.1}$$

$$\frac{dC_i(t)}{dt} = \frac{\beta_i}{\Lambda} N(t) - \lambda_i C_i(t), \quad i = 1, \ldots, I \tag{5.2}$$

We have explored two methods of overcoming the stiffness problem associated with these equations.

The first is to write the prompt neutron equation as:

$$\frac{dN(t)}{dt} = \omega(t)\, N(t) \tag{5.3}$$

where $\omega(t)$ is a time-dependent, instantaneous reactor frequency.

Differentiating (5.1) and (5.3), and introducing the effective decay constant:

$$\lambda_e(t) \equiv \frac{\sum_{i=1}^{I} \lambda_i^2 C_i(t)}{\sum_{i=1}^{I} \lambda_i C_i(t)} \tag{5.4}$$

and solving for $\omega(t)$ yields

$$\omega(t) = \frac{\frac{d\rho(t)}{dt} + \lambda_e(t)\rho(t) + \sum_{i=1}^{I} \beta_i \left(\lambda_i - \lambda_e(t)\right)}{\Lambda \left[\frac{\dot{\omega}(t)}{\omega(t)} + \omega(t) + \lambda_e(t)\right] + \left(\beta-\rho(t)\right)} \tag{5.5}$$

where $\rho(t)$ is the total reactivity present at time, t.

Thus, substituting (5.3) into (5.1), solving for N(t), and using the result to eliminate N(t) from (5.2) leads to

$$\frac{dC_i(t)}{dt} = \frac{\beta_i}{\omega\Lambda + \beta - \rho(t)} \sum_{j=1}^{I} \lambda_j C_j(t) - \lambda_i C_i(t), \quad i = 1, \ldots, I \tag{5.6}$$

The above equations represent an I-dimensional system of differential equations with time-dependent coefficients. They can be time-discretized by rewriting them as

$$\frac{dC_i(t)}{dt} = \left[\frac{\beta_i \theta}{\omega_{n+1}\Lambda + \beta - \rho_{n+1}} \sum_{j=1}^{I} \lambda_j C_j^{(n+1)} - \theta \lambda_i C_i^{(n+1)} + \right.$$

$$\left. \frac{\beta_i (1-\theta)}{\omega_n \Lambda + \beta - \rho_n} \sum_{j=1}^{I} \lambda_j C_j^{(n)} - (1-\theta)\, \lambda_i C_i^{(n)} \right] t \; ; \; t_n \le t \le t_{n+1} \tag{5.7}$$

where subscripts and superscripts (n) and (n+1) specify that the time dependent quantities so labelled are to be evaluated at t_n or t_{n+1}, and where θ is a user-specified averaging parameter. (Taking $\theta = 0$ leads to a fully explicit scheme; $\theta = 1$ gives a fully implicit method, and $\theta = \frac{1}{2}$ is the Crank-Nicholson approximation.)

Integrating Eq. (5.7) from t_n to t_{n+1} leads to a set of equations relating the $C_i^{(n+1)}$ to the $C_i^{(n)}$. Because of their simple structure, these are analytically invertable. The final result is a one-step formula for the delayed neutron precussors:

$$C_i^{(n+1)} = \frac{1 - (1-\theta)\lambda_i \Delta_n}{1 + \theta \Delta_n \lambda_i} C_i^{(n)} +$$

(5.8)

$$+ \frac{\sum_{j=1}^{I} \frac{\lambda_j [1 - (1-\theta)\lambda_j \Delta_n] \theta C_j^{(n)}}{(1+\theta\Delta_n \lambda_i)(1+\theta\Delta_n \lambda_j)} + \frac{(1-\theta)(\omega_{n+1}\Lambda + \beta - \rho_{n+1})}{1+\theta\Delta_n \lambda_i} \frac{N^n}{\Lambda}}{\omega_{n+1}\Lambda + \beta - \rho_{n+1} - \sum_{i=1}^{I} \frac{\lambda_j \theta \Delta_n \beta_j}{1+\theta\Delta_n \lambda_j}} \beta_i \Delta_n$$

for i = 1, . . . , I.

Note that, in this final form, Eqs. (5.3) and (5.1) have been used to express a sum $\Sigma_i \lambda_i C_i^{(n)}$ in terms of $N^{(n)}$. Equations (5.4), (5.5) and (5.8) form a complete system of equations that can be solved iteratively for ω^{n+1} and $C_{i,}^{n+1}$, i = 1, . . . , I, assuming that ρ_{n+1} is known.

Then, equation (5.3) can be solved for N^{n+1}, assuming knowledge of N^n:

$$N^{n+1} = N^n \exp\left(\int_{tn}^{t_{n+1}} \omega(t)dt\right) \tag{5.9}$$

The integral in equation (5.8) can be calculated explicitely using (5.5) and making the following approximation,

$$\Lambda \left[\frac{\dot{\omega}(t)}{\omega(t)} + \omega(t) + \lambda_e(t)\right] << \beta - \rho(t) \tag{5.10}$$

which is quite accurate for operational transients.

Summarizing, the following approximation are made in this approach.

(1) In the calculation of ω(t) for use in (5.8)

$$\frac{\dot{\omega}(t)}{\omega(t)} << \omega(t) + \lambda_e(t) + \frac{\beta - \rho(t)}{\Lambda}$$

(2) In the calculation of $\int_{t_n}^{t_{n+1}} \omega(t)dt$, approximation (5.10) is used.

(3) The delayed neutron equations are time-discretized.

(4) $\rho(t)$ and $C_i(t)$ are assumed linear in $t\varepsilon[t_n, t_{n+1}]$.
(This is consistent with approximation (3)).

The second approach to eliminating stiffness from the point kinetics equations is a modification of the method suggested in reference (10).

The kinetic equations are written as (5.1) and (5.2), and as in the first method, Eq. (5.2) is transformed into Eq. (5.6). Defining, the source

$$S(t) = \sum_{j=1}^{I} \lambda_j C_j(t) \tag{5.11}$$

we can rewrite (5.1) as

$$\frac{dN(t)}{dt} = \frac{\rho(t)-\beta}{\Lambda} N(t) + S(t) \tag{5.12}$$

As in the first approach, equation (5.6) is discretized in time, and equation (5.12) is rewritten (in view of (5.3) as

$$\omega(t) = \frac{\rho(t)-\beta}{\Lambda} + \frac{S(t)}{N(t)} \tag{5.13}$$

The discretized equation (5.8) along with (5.11), (5.12) and (5.13) form a complete set that can be solved iteratively to obtain the power behavior in time. It should be noted that equation (5.12) can be solved analytically if it is assumed that $\rho(t)$ and $C_i(t)$ are linear in $[t_n, t_{n+1}]$, an approximation consistent with the finite differencing of equation (5.6).

The difference in the two approaches is the fact that the prompt neutron equation is not included in the iteration for $\omega(t)$ in the first method,

whereas the second method requires its inclusion.

To summarize: the following approximations are made for the second method.

(1) Time discretization of the delayed neutron precussor equation.

(2) $\rho(t)$ and the $Ci(t)$ are assumed to be linear in $t \in [t_n, t_{n+1}]$. (This approximation is consistent with (1)).

5.2 Numerical Results

Two example problems are presented in order to demonstrate the accuracy of the two methods.

The first problem is a relatively fast ramp reactivity insertion of reactivity of 10¢/sec. for 8 sec. Thus the final core reactivity is 80¢. The reference solution was obtained from Ref. (10). All powers are normalized to unit initial values. Table (5-1) shows the results

Time (s)	Ref.	1st Method (% Rel. Er.)	2nd Method (% Rel. Er.)
2	1.3382	1.3386(.0299)	1.3382(0.)
4	2.2283	2.2311(.1257)	2.2286(.0135)
6	5.5815	5.6157(.6127)	5.5846(.0555)
8	4.2781E+01	4.5024E+01(5.2430)	4.2996+E01(.5026)

Table (5-1) Test of Methods (1) and (2) for 10¢/sec Ramp Insertion; Normalized Power vs Time.

The reference was calculated using $\Delta t = 10^{-4}$ sec. The other two calculation were performed with $\Delta t = 0.1$ sec. Best accuracy was found using θ's

of 1.0 and .5 respectively. The computational effort for the two methods was .03 cpu sec. per real sec. and .07 cpu sec/simulated sec. respectively.

The second example problem is a ramp reactivity insertion at the operational level of 5mβ/sec for 5 sec. The reference calculation was taken from Ref. (11) and was performed with $\Delta t=10^{-4}$ sec. The results are shown in Table (5.2). (Power is in KW.)

Time (s)	Ref.	1st Method (% Rel. Er.)	2nd Method (% Rel. Er.)
1	1005.90	1005.75(-.015)	1005.86(-.004)
2	1013.02	1012.78(-.024)	1013.01(-.001)
3	1021.23	1020.91(-.031)	1021.22(-.001)
4	1030.45	1030.06(-.038)	1030.44(-.001)
5	1040.65	1040.21(-.042)	1040.65(0.0)

Table (5-2) Tests of Methods (1) and (2) for 5mβ/sec Reactivity Ramp Insertion; Power in Kilowatts vs Time

Both methods were run with Δt= 1sec. Any time step smaller than 1sec. reproduced the reference solution correct to the first decimal digit. The computational times were such that the first method ran 250 times and the second method 85 times faster than real time.

Comparing the two methods we see that the second method, although more accurate, is computationally more expensive. For an operational transient, the first method gives acceptably accurate results and runs much faster than real time.

REFERENCES

1. A.F. Henry, O.A. Adekagbe, W.H. Francis, I.S. Muhtaseb, A.C. Onyemalcho, T.A. Taiwo and E. Tanlar, "Continued Development of Nodal Methods for Reactor Analysis", M.I.T. Energy Laboratory Report No. MIT-EL-85-003; March 1985.

2. Ediz Tanker, "Matching the Solution of the Transport Equation With Diffusion Theory Using Average Discontinuity Factors", Nucl. Eng. MS Thesis, Department of Nuclear Engineering, MIT, Cambridge, Mass. (1986).

3. A.F. Henry, Nuclear-Reactor Analysis, M.I.T. Press, Cambridge, Mass., 1975.

4. D.L. Delp, D.L. Fischer, J.M. Harriman and M.J. Stedwell, "FLARE: A Three-dimensional Boiling Water Simulator", General Electric Co. Report GEAP-4598 (1964).

5. S. Borrensen, "A Simplified, Coarse-Mesh, Three-Dimensional Diffusion Scheme for Calculating the Gross Power Distribution in A Boiling Water Reactor", NUC. Sci. Eng. 44 37 (1971).

6. L.A. Hageman and C.J. Pfeifer, "The Utilization of the Neutron Diffusion Program PDQ-5," WAPD-TM-395, Bettis Atomic Power Laboratory, Jan. 1965.

7. T.B. Fowler, D.R. Vondy, and G.W. Cunningham, "Nuclear Reactor Core Analysis Code: CITATION," ORNL-TM-2406, Oak Ridge National Laboratory 1969.

8. K.S. Smith, "An Analytic Nodal Method for Solving the Two-Group, Multi-dimensional, Static and Transient Neutron Diffusion Equations", Nucl. Eng. Thesis, Department of Nuclear Engineering, MIT, Cambridge, Mass. (1979).

9. A.F. Henry, "Few-Group Approximations based on a Variational Principle", Nucl. Sci. Eng. 27, 493-510 (1967).

10. Yung-An Chao and Anthony Attard, "A Resolution of the Stiffness Problem of Reactor Kinetics", Nuc. Sci. Eng. 90 40-46 (1985).

11. J.A. Bernard, "Development and Experimental Demonstration of Digital Closed-Loop Control Strategies for Nuclear Reactors", MIT-NE Thesis, (1984).